Running head: ELA of ecological communities

Energy landscape analysis elucidates the multistability of ecological communities across environmental gradient

Kenta Suzuki[1*], Shinji Nakaoka[2,3], Shinji Fukuda[3-6] and Hiroshi Masuya[1]

* Corresponding author: kenta.suzuki.zk@riken.jp, +81-0298369137

1. Integrated Bioresource Information Division, BioResource Research Center, RIKEN, 3-1-1 Koyadai, Tsukuba, Ibaraki 305-0074, Japan.

2. Laboratory of Mathematical Biology, Faculty of Advanced Life Science, Hokkaido University, Kita-10 Nishi-8, Kita-ku, Sapporo, Hokkaido 060-0819, Japan.

3. PRESTO, Japan Science and Technology Agency, 4-1-8 Honcho, Kawaguchi, Saitama 332-0012, Japan.

4. Institute for Advanced Biosciences, Keio University, 246-2 Mizukami, Kakuganji, Tsuruoka, Yamagata 997-0052, Japan.

5. Intestinal Microbiota Project, Kanagawa Institute of Industrial Science and Technology, 3-25-13 Tonomachi, Kawasaki-ku, Kawasaki 210-0821, Kanagawa, Japan.

6. Transborder Medical Research Center, University of Tsukuba, 1-1-1 Tennodai, Tsukuba, Ibaraki 305-8575, Japan.

Abstract

Compositional multistability is widely observed in multispecies ecological communities. Since differences in community composition often lead to differences in community function, understanding compositional multistability is essential to comprehend the role of biodiversity in maintaining ecosystems. In community assembly studies, it has long been recognized that the order and timing of species migration and extinction influence structure and function of communities. The study of multistability in ecology has focused on the change in dynamical stability across environmental gradients, and was developed mainly for low-dimensional systems. As a result, methodologies for studying the compositional stability of empirical multispecies communities is not well developed. Here, we show that models previously used in ecology can be analyzed from a new perspective - the energy landscape - to unveil compositional stability of multispecies communities in observational data. To show that our method can be applicable to real-world ecological communities, we simulated the assembly dynamics driven by population level processes, and show that results were mostly robust to different simulation conditions. Our method reliably captured the change of the overall compositional stability of multispecies communities over environmental change, and indicated a small fraction of community compositions that may be a channel for transition between stable states. When applied to mouse gut microbiota, our method showed the presence of two alternative states with change in age, and suggested the multiple mechanism by which aging impairs the compositional stability of the mouse gut microbiota. Our method will be a practical tool to study the compositional stability of multispecies communities in a changing world, and will facilitate empirical studies that integrate the concept of multistability developed in different fields of ecology in the past decades.

Keywords

Community assembly, Compositional stability, Historical contingency, Multistability, Alternative stable states, Regime shift, Presence/absence data, Markov network, Pairwise maximum entropy model, Principle of maximum entropy, Stability landscape, Energy landscape

Introduction

It has been recognized that the order and timing of species migration and extinction during community assembly influence structure (Drake 1991, Fukami and Morin 2003) and function (Fukami et al. 2010, Jiang et al. 2011) of communities, resulting in multistability (also known as alternative stability) of different community compositions (Fukami 2010, Fukami 2015). Multistability in community assembly dynamics have many empirical examples (see, e.g., review by Schlöder et al. 2005). For example, in aquatic microbial communities, Drake (1991) showed the effect of the sequences of species invasions on final community composition. More recently, also with aquatic microbial communities, Pu & Jiang (2015) found that alternative community states were maintained for many generations despite frequent dispersal of individuals among local communities. Particularly in the field of microbial ecology, the recent development of next-generation sequencing technology has made it possible to comprehensively study community structures (Caporaso et al. 2010, Ding and Schloss 2014, Thompson et al. 2017, Bolyen et al. 2019). This development led to recognition of the strong association between composition and function of microbial communities that is essential for the maintenance of host organisms or physical environment (Costello et al. 2012, Widder et al. 2016, Sommar et al. 2017). For example, in the animal intestine there is a phenomenon called dysbiosis in which function is severely impaired due to infection or other causes (Carding et al. 2015). One example would be *C. difficile* infection (CDI) (Kelly and LaMont 2008, Britton and Young 2014). CDI is established when *C. difficile* invades and successfully colonizes a gut microbiota that has been disrupted from its normal balance, e.g., by antibiotics. The normal microbiota is resistant to *C. difficile* colonization whereas it is significantly altered when *C. difficile* successfully colonizes the intestine. There would be at least two community compositions (with or without *C. difficile*) that are stable at the same environmental conditions. In this case, transplantation of the normal microbiota can effectively restore the infected microbiota back to normal (Bakken et al. 2011). However, simply implanting a desirable microbiota is not a universal method for its establishment (Rilling et al. 2015, Castledine et al. 2020), and a more systematic methodology is required (Mueller and Sachs 2015, Sbahi and Di Palma 2016, Toju et al. 2020). Thus, there is growing momentum for developing a methodology to account for compositional stability in multispecies communities that can provide a basis for predicting, preventing and controlling large-scale shifts in community compositions.

Studies on multistability in ecology have been mainly developed for low dimensional systems (May 1977, Scheffer et al. 2001, Beisner et al. 2003). One typical example is the relationship between the abundance of phytoplankton and plant species with

phosphorus concentration in lake systems (Scheffer and Jeppsen 2007): there are contrasting conditions represented by low and high algal density, and a gradual shift of phosphorus concentration triggers a rapid transition known as a catastrophic regime shift. These studies raise two important challenges regarding the analysis of compositional stability in multispecies communities, which we focus on here. First, the potential landscape description, called "ball and cup diagram", has been frequently used to explain the stability of low dimensional systems (see, e.g., Scheffer et al. 2001), but how should it be interpreted when the system cannot be simplified to a few dimensions? As a solution, we introduce the concept of the *stability landscape* in this paper. The term has already been used in some studies. For example, Walker et al. (2004) used the term to refer to the ball and cup diagram itself. Recent studies implement this idea to study the stability of microbial communities by projecting their abundance data to a continuous potential landscape with a few dimensions (Gibson et al. 2017, Shaw et al. 2019). In contrast to the previous definition, in this paper we define the stability landscape as a structure that governs compositional stability of ecological communities (Figure 1). The stability landscape maps out overall compositional stability of an ecological community as a graph with a set of community compositions and transition paths between them. Such a view has already been introduced in some experimental (Weatherby et al. 1998, Law et al. 2000, Warren et al. 2003) and theoretical studies (Law and Morton 1993, Capitan et al. 2011), but our goal here is to develop a methodology by which we can study stability landscapes from observational data. Second, it is also important to capture changes of stability landscape in response to environmental changes. For example, Lahti et al. (2014) showed that there are some taxa in human gut microbiota that show contrasting abundances according to age and lead to a shift of microbial composition during middle to old age. In this case, age was regarded as a dominant parameter of the intestinal environment and the key to transition between two contrasting states. However, given that the composition of microbiota may shift due to causes other than aging, such as infections (Kelly and LaMont 2008, Costello et al. 2012), it would be important to address changes in the overall compositional stability rather than the stability of two contrasting states.

To define the stability landscape of multispecies communities addressing the points described above, we introduce an energy landscape analysis (Becker and Karplus 1997, Wales et al. 1998, Watanabe et al. 2014a) incorporating an extended pairwise maximum entropy model. The extended pairwise maximum entropy model is a mix up of two models that have previously been used in ecology. One is the species distribution model known as MaxEnt (Philips et al. 2004, 2006), and the other is the pairwise

maximum entropy model (Schneidman et al. 2006; in ecology it is introduced as Markov network, see, e.g., Azaele et al. 2010, Araujo et al. 2011, Harris 2015). MaxEnt was developed around a model that predicts species distribution from environmental conditions, and by using the maximum entropy principle, it gives the least biased distribution estimates given prior knowledge such as observational data (Jaynes 1982, Harte and Newman 2014). While MaxEnt is known to give more accurate predictions relative to comparable models (Elith et al. 2006), it is unable to handle co-occurrence information that signals biotic interactions as well as shared environmental preferences between species (Kissling et al. 2012, Ockendon et al. 2014, Thuiller et al. 2015, Barner et al. 2018, Freilich et al. 2018). When community-level occurrence data is available, such information can be used to obtain more accurate predictions for species distribution (Meier et al. 2010, Leach et al. 2016, Barbaro et al. 2019). We used the pairwise maximum entropy model to fulfill this role. The pairwise maximum entropy model is obtained by applying the maximum entropy principle to co-occurrence information (Azaele et al. 2010). The model has already been used to predict species distribution and/or to detect signals of biotic interactions behind co-occurrence data (Azaele et al. 2010, Araujo et al. 2011, Harris 2016). Integration of MaxEnt and the pairwise maximum entropy model has been attempted in one previous study, aimed at improving the accuracy of species distribution predictions and refining the estimation of biotic interactions under environmental heterogeneity (Clark et al. 2018), but the purpose of introducing the integrative model here is different.

By introducing the energy landscape analysis, we show how we can use the pairwise maximum entropy models to study the stability landscape of multispecies communities. While the stability landscape represents the actual compositional stability driven by population dynamics, the energy landscape is its approximation based on the maximum entropy principle given observational data. Energy landscape analysis is the analysis of topological and connection attributes of a weighted network defined as the energy landscape (Watanabe et al. 2014a), and informs how it constrains the compositional dynamics just as the ball and cup diagram does for low dimensional systems. Energy landscape analysis has its origins in the study of molecular dynamics (Becker and Karplus 1997, Wales et al. 1998) and was recently proposed as a data analysis method for neuroscience (Watanabe et al. 2014a,b, Ezaki et al. 2017, Watanabe & Rees 2017, Ezaki et al. 2018). Watanabe et al. (2014a) described the activity of multiple brain regions as binary vectors to show that the activity patterns of the resting brain are attracted to a small number of attractive states, and these states are hierarchically structured. This was done by 1) defining a set of unique activity patterns (network nodes) and connections between them as the transition path between different activity

patterns (network links), 2) weighting each activity pattern by *energy* given by a pairwise maximum entropy model, and 3) analyzing the connection attributes of the weighted network, i.e., energy landscape. We attempt to fully ground the concept of energy landscape analysis in an ecological context, and, by introducing the extended pairwise maximum entropy model, add methodological advancement to account for the shift of stability landscapes across environmental changes. This will be a practical tool to study the compositional stability of multispecies communities in a changing environment, and will open up the possibility of empirical studies that integrate the concept of compositional multistability in multispecies communities and regime shifts developed mainly for low-dimensional systems. To show that our proposed method can be applicable to real-world ecological communities, we simulated the assembly dynamics driven by population level processes, and show that the features characterizing the stability landscape can be effectively inferred by pairwise maximum entropy models with the help of energy landscape analysis.

This paper is organized as follows. In the next section, we thoroughly explain our methodology, as well as the setup of a Lotka-Volterra (LV) model that we used for benchmarking. We then present a demonstrative analysis showing how a stability landscape of the LV model was studied. We also benchmarked our methodology for multiple independent data sets obtained from different simulation conditions. Finally, to demonstrate the application to a real-world community, we applied our methodology to the murine gut microbiota (Nakanishi et al. submitted). We found two alternative stable states and revealed how change in their relative stability is affected by age in the presence of background species relationships.

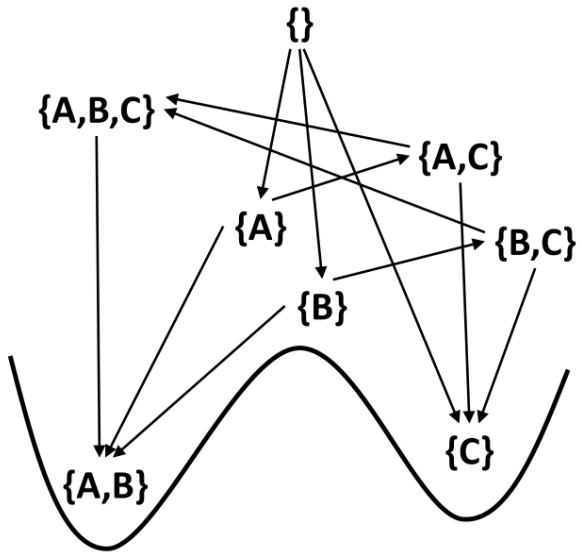

Figure 1. Example of a stability landscape for a conceptual three-species system. Two species, A and B, are cooperative, and these species can exclude species C if both of them are present. On the other hand, C excludes either A or B as long as they are present alone. Arrows indicates the transition of community composition when species always joins the system one-by-one. Transition from {A, C} (or {B, C}) to {A, B, C} is only valid when {B} ({A}) appears before exclusion occur. Here, both composition {A, B} and {C} is a stable state correspond to the bottom of the valley in the ball and cup diagram. The remaining six transient states can be divided into those in the basin of either stable state (in terms of the result of competition among the species present) and those on the ridge between the basins (which can transition to either of the stable states depending on the subsequent recruitment). Thus, the potential landscape represented as a smooth curve in the ball and cup diagram is embodied as a network connecting different species compositions when capturing compositional stability.

Materials and Methods

Definition of state space

By formalizing the concept of stability landscape, we obtain a definition of state space for energy landscape. We define a community composition σ as a binary vector, i.e., a string of 0's (absence) and 1's (presence), whose length S is the total number of species. Thus, there is a total of 2^S unique community compositions, which are the nodes of the energy landscape. We denote a community composition of kth sample ($k \in \{0,1,\dots,2^{S-1}\}$) as $\sigma^{(k)} = (\sigma_1^{(k)}, \sigma_2^{(k)}, \dots, \sigma_S^{(k)})$, where $\sigma_i^{(k)} \in \{0,1\}$ is the presence absence status of the ith species. Then, we define the links that connect community compositions under the assumption that community compositions change in a stepwise manner, i.e., two community compositions are adjacent by a link only if they take the opposite status (i.e., 0/1) for just one species. Under this assumption, the community compositions form a regular network in which each node has S links, which is the state space for an energy landscape.

Pairwise maximum entropy models and Energy landscape

The next step is to assign *energy* to each community composition and impose the potential structure to the state space. In order to do so, we first need to introduce the pairwise maximum entropy models.

The extended pairwise maximum entropy model determines probability of the occurrence of community composition $\sigma^{(k)}$ in an environmental condition $\varepsilon =$

$(\varepsilon_1, \varepsilon_2, \ldots, \varepsilon_M)$, which is an array of continuous values representing environmental factors such as resource availability, pH, temperature, or age of host organism:

$$P(\sigma^{(k)}|\epsilon) = e^{-E(\sigma^{(k)},\varepsilon)}/Z, \quad (1)$$

$$E(\sigma^{(k)}, \varepsilon) = -\sum_{i=1}^{S} h_i \sigma_i^{(k)} - \sum_{j=1}^{S} \sum_{i=1}^{M} g_{ij} \varepsilon_i^{(k)} \sigma_j^{(k)} - \sum_{i=1}^{S} \sum_{j=1, j\neq i}^{S} J_{ij} \sigma_i^{(k)} \sigma_j^{(k)} /2. \quad (2)$$

Here, $E(\sigma^{(k)}, \epsilon)$ is defined as the energy of community composition $\sigma^{(k)}$, and $Z = \sum_{k=0}^{2^{S-1}} e^{-E(\sigma^{(k)},\varepsilon)}$. (3)

It is worth noting that we label $E(\sigma^{(k)}, \epsilon)$ as energy simply because of the terminology for the same equation in statistical physics (Brush 1967, Azaele et al. 2010). In ecology, it is nothing but an exponent in eq.(1) and is an indicator of how often a community composition is likely to be observed. It should be emphasized that it does not correspond in any way to the physical form of energy used in the ecological studies. Parameters in eq.(2) are h_is, J_{ij}s and g_{ij}s, which are elements of a vector $h = (h_1, h_2, .., h_S)$ and matrix $J = (J_{ij})_{i=1,2,\ldots,S;j=1,2,\ldots,S}$ and matrix $g = (g_{ij})_{i=1,2,\ldots,M;j=1,2,\ldots,S}$, respectively. As a model for an ecological community, h_i is interpreted as the net effect of unobserved environmental factors, which may favor the presence ($h_i > 0$) or absence ($h_i < 0$) of species i. On the other hand, g_{ij} represents the effect of the ith (observed) environmental factor on the occurrence of the jth species. Moreover, each species is coupled to all others in a pairwise manner through J_{ij}s, and correspondingly, $J_{ij} > 0$ favors the co-occurrence of species i and j and $J_{ij} < 0$ disfavors the co-occurrence of species i and j. Obviously, the extended pairwise maximum entropy model can be reduced to the pairwise maximum entropy model (Azaele et al. 2010, Araujo et al. 2011, Harris 2015) with,

$$E(\sigma^{(k)}) = -\sum_{i=1}^{S} h_i \sigma_i^{(k)} - \sum_{i=1}^{S} \sum_{j=1, j\neq i}^{S} J_{ij} \sigma_i^{(k)} \sigma_j^{(k)} /2, \quad (4)$$

if the effect of environmental condition can be neglected. Eq. (2) and (4) are based on pairwise interactions. Thus, it is implicitly assumed that all higher-order occurrence patterns are well-captured by the information encapsulated in the first two moments (Azaele et al. 2010). This is relaxed by including the high order terms in these equations. However, such extension would increase the dataset size required to obtain enough predictive performance (Nguyen et al. 2017).

As the pairwise maximum entropy models assign *energy* to each community composition in state space, we obtain an energy landscape. The energy represents the directionality of the transition between community compositions. For each pair of two adjacent nodes (say, $\sigma^{(k)}$ and $\sigma^{(k')}$), let $P(\sigma^{(k)}) < P(\sigma^{(k')})$, i.e., $E(\sigma^{(k)}) > E(\sigma^{(k')})$, the transition of community compositions is more likely to occur from $\sigma^{(k)}$ to $\sigma^{(k')}$ than

$\sigma^{(k')}$ to $\sigma^{(k)}$. Since such a local transition rule governs the transition dynamics as in a chain rule, the energy landscape determines the directionality of overall compositional dynamics. We expect that this could be an approximation of the stability landscape.

We are now ready to explain how we obtain the energy landscape for an observational dataset. We assume that we have a dataset containing the community compositions of N samples (Fig. 2A, B). We denote the community composition of samples as an $S \times N$ matrix $X = (x_1, x_2, \dots, x_N)$ and $x_i \in \{\sigma^{(1)}, \sigma^{(2)}, \dots, \sigma^{(2^S)}\}$ (Fig. 1B). If available, we denote the environmental condition of N samples as $M \times N$ matrix $Y = (y_1, y_2, \dots, y_N)$, where local environmental condition $y_i = \varepsilon^{(i)} = (\varepsilon_1^{(i)}, \varepsilon_2^{(i)}, \dots, \varepsilon_M^{(i)})$ represents the environmental factors of the ith sample (Fig. 2B). We regard the X and Y pair as observational data. The maximum likelihood estimates of h, J and g can be obtained by a gradient descent for the pairwise maximum entropy model (eq.(4)) or stochastic approximation method for the extended pairwise maximum entropy model (eq.(2)) as described in *Parameter fitting* (Fig. 2C). Since these equations are derived from the maximum entropy principle, probability distribution of community compositions with these parameters is the least biased estimate given the observational data (Jaynes 1982, Harte and Newman 2014). In other words, the probability distribution satisfies the constraints imposed by the observational data while maximizing the remaining uncertainty. This is a reasonable and well-verified (Shipley et al. 2006, Elith et al. 2006, Franklin 2009, Parisien and Moritz 2009, Harte 2011, Staniczenko et al. 2017, Clark et al 2018) assumption to estimate the probability of the occurrence of community composition that is not actually observed. At the same time, these equations determine the energy of all community compositions, and provide an energy landscape by imposing a potential structure to the state space.

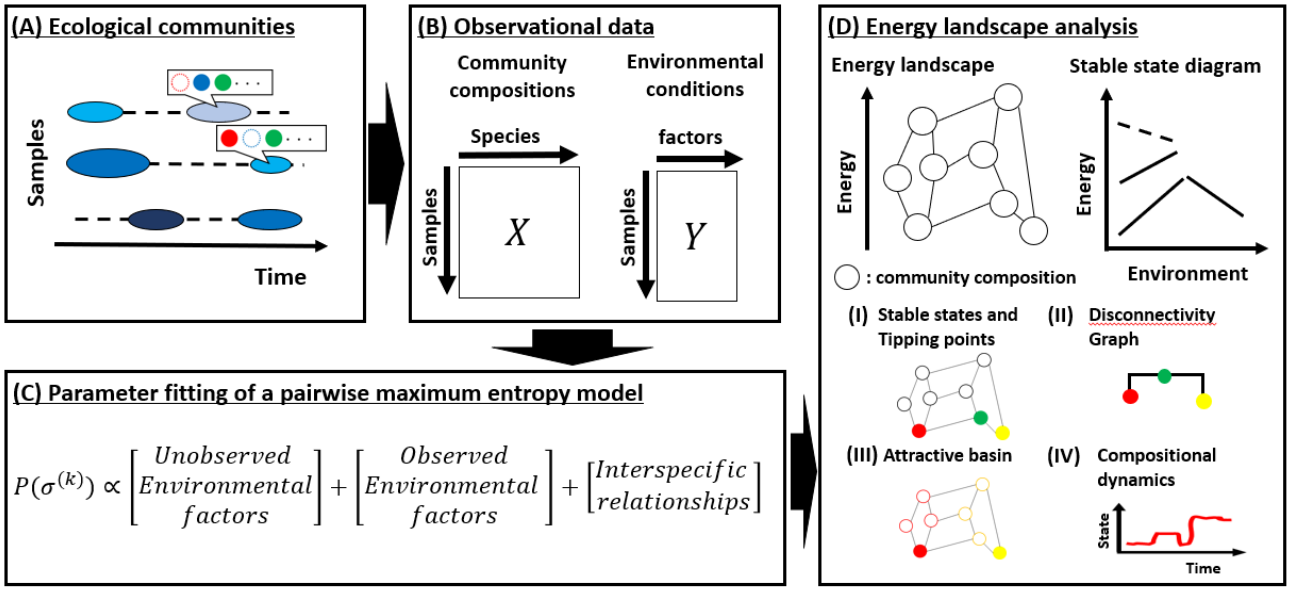

Figure 2. Illustrative explanation of our approach. (A) we assume that the dataset includes occurrence of species in local communities sampled from multiple targets (e.g., sites, hosts) and/or timepoints, with possibly accompanying values representing local environmental condition (environmental factors) (in the illustration, circles and filled circles show species that are absent from or present in a local community, and colors and size of ellipses represent differences in environmental condition). (B) dataset is converted to matrices of presence/absence status, and environmental factors (if they are available). (C) these matrices are used to fit parameters in a pairwise maximum entropy model. Here, $P(\sigma^{(k)})$ is the probability of a community state $\sigma^{(k)}$ (see Materials and Methods for the detail). (D) the fitted pairwise maximum entropy model specifies an energy landscape which is a network with nodes representing community states and links representing transitions between community compositions. Its change over environmental conditions can be described as a stable state diagram. Energy landscape analysis, acknowledges (I) the stable states (red and yellow filled-circles) and tipping points (green filled-circle), (II) disconnectivity graph summarizing the hierarchical relationships between the stable states and tipping points, (III) attractive basin of stable states (red and yellow circles indicate attractive basins of the two stable states), (IV) compositional dynamics constrained by the energy landscape.

Energy landscape analysis

Energy landscape analysis is an analysis on the topological and connection attributes of an energy landscape (Fig. 2D). Below, we show how to identify its key components and explain how they can help us to understand the structure of a stability landscape. We will use the term "node" in the same sense as one community composition.

Energy minima - We identify energy minima of an energy landscape as stable states of a stability landscape (red and yellow filled circles in Fig. 2D). The local minima have the lowest energy compared to all neighboring nodes, and thus constitute end-points when assembly processes are completely deterministic (i.e., when transition of community compositions always go down the energy landscape). Presence of multistability can be identified as multiple energy minima within an energy landscape. Since an energy minimum is a node with energy less than all S neighboring nodes, we exhaustively examined whether each of the 2^S nodes are local minima. The same idea has already been described in Azaele et al. (2010) but they only mentioned it briefly in their analysis on a plant community distribution.

Attractive basin - The attractive basin (red and yellow circles in Fig. 2D) is the set of community compositions that eventually reach one distinct stable state when assembly processes are completely deterministic, and thus identified according to the stable state that it converges to. The attractive basin to which a community composition belongs to is determined by a steepest descent method as follows. First, we selected a node i in the energy landscape. If the selected node is not a local minimum, we moved to the node with the lowest energy value among the nodes adjacent to the current node. We repeated moving downhill in this manner until a local minimum is reached. The initial node i belongs to the basin of the finally reached local minimum. We ran this procedure for each of 2^S nodes except for local minima.

Disconnectivity graph, energy barriers and tipping points - A disconnectivity graph is a tree diagram that summarizes the structure of an energy landscape (Fig. 2D). It is important in that it informs us about the hierarchical relationships among stable states. Terminal leaves of the tree represents the stable states and their vertical positions represent their energy values. Those of the branches represent the height of the energy barrier that separates the stable states belonging to the two branches. Here, the community composition connecting two branches is a tipping point. Tipping point is the lowest part of the ridge between two basins (green filled-circles in Fig. 1D). When we consider the transition from a stable state $\sigma^{(A)}$ to the other stable state $\sigma^{(B)}$ ($\sigma^{(A)} \rightarrow \sigma^{(B)}$), the height of the energy barrier is calculated as the energy of the tipping point minus that of $\sigma^{(A)}$. Similarly, the height of the energy barrier for $\sigma^{(B)} \rightarrow \sigma^{(A)}$ is calculated as the energy of the tipping point minus that of $\sigma^{(B)}$. Thus, the directionality of the transition between two stable states is typically asymmetrical and transitions with smaller energy barriers occur more frequently than the opposite direction. Tipping points can be obtained by checking connectivity of an energy landscape while changing

an energy threshold value as follows. First, we set an energy threshold value, denoted by E_{th}, to the energy value of the node that attained the second highest energy value among community compositions. Second, we removed the node (and the links connected to the node) with the highest energy value. At this point, the node whose energy is E_{th} turns to the highest energy state. Third, we checked whether each pair of stable states was connected in the reduced network. Forth, we lowered E_{th} to the second highest energy value again. Then, we repeated the second to forth steps, that is, removal of the nodes and links, checking for connectivity between local minima, and lowering of E_{th}, until all the local minima were isolated. During this process, for each pair of stable states, we recorded a community composition having the lowest E_{th} value below which the two stable states were disconnected. Practically, in some cases, we need to filter out some stable states because they may have been detected incorrectly. Throughout this paper, we pruned stable states whose shallowest energy barrier is 20% lower than the highest energy barrier among all energy barriers across the energy landscape.

Stable state diagram – A stable state diagram unfolds the energy of stable states and tipping points in disconncectivity graphs over environmental conditions (Fig. 2D). It maps out how an energy landscape changes in response to environmental changes. A stable state (and tipping point) is represented as a line segment that indicates a range of environmental conditions in which it is identified. Typically, we identify stable states as solid lines and tipping point as dashed lines.

Numerical simulations - We carried out numerical simulations to generate transition sequences of community compositions constrained by an energy landscape, and we refer to these simulations as emulated compositional dynamics (Fig. 2D). We employed the heat-bath (also known as Gibbs sampling) method (Gilks et al. 1996) as follows. First, we selected an initial community composition. Then, in each time step, a transition from the current community composition $\sigma^{(k)}$ to one of its S adjacent community composition $\sigma^{(k')}$, selected with probability $1/S$, was attempted ($\sigma^{(k)}$ and $\sigma^{(k')}$ differs only with respect to the presence/absence status of one of S species). The transition to the selected community composition took place with probability $e^{-E\left(\sigma^{(k')}\right)}/(e^{-E(\sigma^{(k)})} + e^{-E(\sigma^{(k')})})$.

By using the algorithm, we collected transition sequences of community compositions between different stable states. We then extracted the community composition having the highest energy in each transition sequence. These compositions are likely to

constitute the *effective boundary* between the basin of stable states on the energy landscape.

Parameter fitting

The maximum likelihood estimate for the model parameters can be obtained by minimizing the discrepancy between the values of the data's sufficient statistics and the corresponding sufficient statistics within the model (Bickel and Doksum 1977, Azaele et al. 2010, Murphy 2012, Harris 2015, Lee and Hastie 2015).

Gradient descent algorithm - For a dataset without observation on environmental conditions, i.e., whose energy is given by eq. (4), a gradient descent algorithm can be applied (Watanabe et al. 2014a,b, Harris 2015, Harris 2016). For a model with parameter h^* and J^*, let the expected probability of species i be $\langle\sigma_i\rangle^* = 1/2^S \sum_{k=1}^{2^S} \sigma_i^{(k)} P(\sigma^{(k)})$ and the co-occurrence be $\langle\sigma_i\sigma_j\rangle^* = 1/2^S \sum_{k=1}^{2^S} \sigma_i^{(k)} \sigma_j^{(k)} P(\sigma^{(k)})$. The parameter h and J can be fitted to the data by iteratively adjusting $\langle\sigma_i\rangle^*$ and $\langle\sigma_i\sigma_j\rangle^*$ toward the mean occurrence and co-occurrence calculated from the observational data, $\langle\sigma_i\rangle$ and $\langle\sigma_i\sigma_j\rangle$. Here, the parameters are updated as

$$h_i^{new} \leftarrow h_i^{old} + \alpha \log\langle\sigma_i\rangle/\langle\sigma_i\rangle^*$$
$$J_{ij}^{new} \leftarrow J_{ij}^{old} + \alpha \log\langle\sigma_i\sigma_j\rangle/\langle\sigma_i\sigma_j\rangle^*$$

at each step. We set the learning rate $\alpha = 0.25$ and the maximum number of iterations $T = 5000$, according to the preliminary analysis where we checked the convergence of model parameters.

Stochastic approximation - The likelihood function of the pairwise maximum entropy model becomes computationally intractable when we need to include environmental condition (as in eq. (2)), because it requires repeating above computations independently for every sample. Therefore, it calls for a different model-fitting algorithm that is computationally more efficient. Here, following Harris (2015), we introduce a *stochastic approximation* (Robbins and Monro 1951, Salakhutdinov and Hinton 2012) for this purpose. This algorithm replaces the intractable computations with tractable Monte Carlo estimates of the same quantities. Despite the sampling error introduced by this substitution, stochastic approximation provides strong guarantees for eventual convergence to the maximum likelihood estimate (Younes 1999, Salakhutdinov and Hinton 2012).

Stochastic approximation (Robbins and Monro 1951, Salakhutdinov and Hinton 2012) estimates the expected values of the sufficient statistics by averaging over a more

manageable number of simulated assemblages during each model-fitting iteration, while still retaining maximum likelihood convergence. The advantage of this algorithm is Z (eq. (3)) does not have to be calculated at each step, which significantly improves computational efficiency. This is due to the use of a heat-bath algorithm that only requires calculating energy of two adjacent community compositions. The procedure iterates the following steps:

1. Set $t = 0$, initial learning rate $\alpha_0 = 0.1$, logistic priors as $p_h = -\tanh(h/2/2)/2$, $p_g = -\tanh(g/2/2)/2$ and $p_J = -\tanh(J/0.5/2)/2$ and initialize parameter values for h, J, g, and the expected sample states $X^*(0) = X$. We set $Y^* = Y$ throughout the calculation.

2. Calculate learning rate α as:

$$\alpha = \alpha_0 \frac{5000}{4999 + t},$$

momentum m as:

$$m = 0.9\left(1 - \frac{1}{0.1t + 2}\right).$$

3. For $x_i^*(t)$ from $i = 1$ to N, run one step heat-bath algorithm based on current parameters (h, J and g): transition from the current community composition $\sigma^{(k)}$ to one of its S adjacent community composition $\sigma^{(k')}$, selected with probability $1/S$, was attempted ($\sigma^{(k)}$ and $\sigma^{(k')}$ differs only with respect to the presence/absence status of one of S species). The transition to the selected state took place with probability $e^{-E\left(\sigma^{(k')}|\mathcal{E}^{(i)}\right)}/(e^{-E(\sigma^{(k)}|\mathcal{E}^{(i)})} + e^{-E(\sigma^{(k')}|\mathcal{E}^{(i)})})$. Here, ($e^{-E(\sigma^{(k)}|\mathcal{E}^{(i)})}$ and $e^{-E(\sigma^{(k')}|\mathcal{E}^{(i)})}$ are given by eq. (4). If transition occurs, the sample state is updated as $x_i^*(t) \leftarrow \sigma^{(k')}$.

4. Subtract the simulated sufficient statistics from the observed ones to calculate the approximate likelihood gradient. Sufficient statistics are calculated as, $SS_1^* = X^*(X^*)^t$ (here, $(X^*)^t$ is the transpose of X^*), and $SS_2^* = (X^*)^t Y^*$. Then, we obtain the difference of sufficient statistics as:

$$\Delta SS_1 = SS_1 - SS_1^*,$$

and

$$\Delta SS_2 = SS_2 - SS_2^*.$$

Here, SS_1 and SS_2 is the corresponding sufficient statistics calculated from actual data (i.e., $SS_1 = XX^t$ and $SS_2 = X^t Y$).

5. Adjust the model parameters to climb the approximate gradient, using a schedule of step sizes as:

$$h_{new} \leftarrow h_{old} + \Delta h_{new},$$
$$J_{new} \leftarrow J_{old} + \Delta J_{new},$$
$$g_{new} \leftarrow g_{old} + \Delta g_{new}.$$

Here,

$$\Delta h_{new} = \alpha G_h + m\Delta h_{old},$$
$$\Delta J_{new} = \alpha G_J + m\Delta J_{old},$$
$$\Delta g_{new} = \alpha G_g + m\Delta g_{old},$$

and,

$$G_h = \frac{\mathrm{diag}(\Delta SS_1) + p_h}{N},$$
$$G_J = \frac{\Delta SS_1 + p_J}{N}|I(S) - 1|,$$
$$G_g = \frac{\Delta SS_2 + p_g}{N},$$

are the approximated likelihood gradients. Here, $I(S)$ is a $S \times S$ identity matrix.

6. Set h_{new}, J_{new}, g_{new}, Δh_{new}, ΔJ_{new} and Δg_{new} as h_{old}, J_{old}, g_{old}, Δh_{old}, ΔJ_{old} and Δg_{old}, respectively. If $t < T$, increment t by 1 and back to 2, else terminate the loop.

Here, the simulations in Step 3 use one step heat-bath algorithm (Gibbs sampling) to generate a community composition distribution based on the model's current parameter estimates. While the subsequent community compositions produced by Gibbs sampling are autocorrelated, this does not prevent convergence to the maximum likelihood estimates (Younes 1999, Salakhutdinov and Hinton 2012). Approximated likelihood gradients in Step 5 match those of gradient descent, except that they are averaged over a set of Monte Carlo samples rather than over all possible community composition. These gradients were augmented with a momentum term (Hinton 2012) and by regularizers based on a logistic prior with location 0 and scale 2.0 (for environmental responses) or 0.5 (for pairwise interactions). We set hyper parameters in this algorithm including maximum number of iteration steps $T = 50000$, according to the preliminary analysis where we checked the convergence of model parameters.

Sample data for demonstration

Competitive Lotka-Volterra model - To test the applicability of our method to community assembly dynamics driven by population level processes, we used the following Lotka-Volterra (LV) competition equation:

$$dx_i = x_i\left(1 - \Sigma a_{ij} x_i + \Sigma b_i \epsilon\right). \quad (5)$$

Here, x_i is the population abundance of species i and it is an element of abundance vector $\vec{x}$. A positive real number a_{ij} represents competitive interactions between species i and j, which is an element of an interaction matrix $A = (a_{ij})$. The diagonal elements of A, i.e., a_{ii}s, represent the intraspecific interactions. The environmental condition is represented by ϵ. It actually can be a vector but we assumed that it is a scalar with a range of $[0, 1]$ throughout our simulation. If we do not consider the environmental variation then $\epsilon = 0$. Response of species i to ϵ is represented by b_i, which is an element of a response vector b. When $\epsilon = 0$, eq. (5) is considered to be one of the simplest multi-species systems whose multistability has already been investigated (Gilpin and Case 1976). In a more general view, LV equations are derived as the continuous limit of individual based models (Wilson et al. 1993) or an approximation of patch dynamic models (Keymer et al. 2000). Therefore, the LV equation-based model will be an important starting point for testing the applicability of our method to real-world ecological communities.

To simulate assembly dynamics, we introduced the processes of *extinction* and *recruitment* into our model. Extinction is a process that reduces the frequency of species fall below a certain threshold (e) to zero and recruitment is an operation to introduce a species that is absent from the system at a propagule size (r). We set $e = 10^{-5}$ and $r = 10^{-4}$ throughout this paper. To simplify the analysis, we set a fixed interval for recruitment $\tau_r = 300$.

In the following manner, we generated a *simulated data set* that characterizes the stability landscape of a LV competition model. First, we generated 20000 empty sites (i.e., $\vec{x}$s such that all elements are zero). The number of species S is fixed throughout the simulation. Thus, it is implicitly assumed that there is a species pool with S species. We assumed that the population dynamics, extinctions and recruitments occur independently among sites. We obtained the numerical solution of the LV equation by the first-order Euler method with $dt = 0.1$. After the first species (randomly selected from the species pool) is added to each site, every τ_r steps, for each site we checked the absent species, randomly select one of them and introduced it with a propagule size r. During these processes, the abundance vector $\vec{x}$ of the LV model is recorded every 10 steps after replacing the abundance of species that falls below e by zero. We interpret $\vec{x}$ as a community composition $\sigma^{(k)}$ by an observational threshold $o = 10^{-3}$, where

abundance is replaced by 1 if $x_i > o$ else 0. Then, time series are interpreted as *assembly sequences* represented by community compositions. The following test for stopping the simulation is applied every τ_r steps before introducing a species; letting $\hat{p}(\sigma^{(k)})$ be the present probability of community compositions of 20000 sites and $\hat{q}(\sigma_i)$ be the same value at τ_r steps ago, for the set of the indices of community compositions K that appeared in records, we calculated the Jansen-Shannon divergence between them as:

$$D_{JS} = \sqrt{\{\sum \hat{p}(\sigma^{(k)}) \log \frac{\hat{p}(\sigma^{(k)})}{\mu_{pq}(\sigma^{(k)})} + \sum \hat{q}(\sigma^{(k)}) \log \frac{\hat{q}(\sigma^{(k)})}{\mu_{pq}(\sigma^{(k)})}\}/2}.$$

Here, $\mu_{pq}(\sigma^{(k)}) = \{\hat{p}(\sigma^{(k)}) + \hat{q}(\sigma^{(k)})\}/2$. The simulation is stopped if $D_{JS} < 0.0001$. We have arranged the numerical simulation procedure to facilitate the determination of stable states. It would be difficult to find an ecological interpretation of this procedure; currently, there are few studies on population-level models aimed at capturing compositional stability of multispecies communities (but see Capitan et al.). It is beyond the purpose of this paper to consider what process should be implemented to reproduce the probability distribution of community compositions in nature.

By using the simulated data set, we identified five features that characterize the stability landscape. Prior to this, we truncated the first five points of the assembly sequence to remove the effect of initial state. To reduce the variation, we calculated the following features for community compositions observed at least more than 20 times. First, we identified the unique community compositions found at the end of each time series as stable states. It is directly comparative to the stable states of energy landscape. Second, we calculated the empirical probability of the occurrence of a community composition $\sigma^{(k)}$ across overall assembly sequences as $\hat{P}(\sigma^{(k)})$. It is comparative to the probability calculated from a pairwise maximum entropy model, $P(\sigma^{(k)})$, which we refer to as the expected probability. Third, we calculated the relative convergence time (RCT) for each community composition. This value indicates relative position of a community composition in a stability landscape with respect to the position of a stable state. It is comparative to the energy of community states; more precisely, we compared it to the rescaled energy $\overline{E}_k$, which takes 0 at a stable state and 1 at a community composition that has highest energy within an attractive basin. RCT is calculated as follows: first, if there are a sub-sequences of the same compositions in an assembly sequence, we removed the redundancy by replacing them with one (i.e., $\{\ldots, \sigma^{(A)}, \sigma^{(B)}, \sigma^{(B)}, \sigma^{(C)}, \ldots\} \rightarrow \{\ldots, \sigma^{(A)}, \sigma^{(B)}, \sigma^{(C)}, \ldots\}$). Then, we rescaled the position of community composition as a value between 0-1. For each community composition, $RCT(\sigma^{(k)})$ is the mean of their rescaled position in all sequences in which they

appeared. Forth, we identified the attractive basin of $\sigma^{(k)}$ as follows: for each community composition $\sigma^{(k)}$, we picked up the end state of the sequences in which it appeared and counted the number of each stable state. We determined that $\sigma^{(k)}$ is in the attractive basin of a stable state to which it is most frequently converged to (if there is more than one such states, it belongs to all of them). It is directly comparative to the attractive basin inferred by the energy landscape. Finally, we calculated the imbalance score (IS) to evaluate how stable states that a community composition converges to is uniquely determined. Similar to determining the attractive basin, for each community composition $\sigma^{(k)}$, we picked up the end state of sequences in which it appeared. Then, we calculated a Gini-Simpson index for the set of stable states as the imbalance score (i.e., $\mathrm{IS}(\sigma) = 1 - \Sigma p_i^*$; here, p_i^* is the relative frequency of stable states). Different from other features, instead of defining a comparative value in energy landscape, we used IS to evaluate the relevance of the hierarchical structure of energy landscape to the actual transition dynamics. For the sake of simplicity, we will refer to the values obtained from a stability landscape as *actual* features, in contrast to the features *inferred* from only a small fraction of simulated data by using the maximum entropy models and the energy landscape analysis. Actual features can only be obtained with the large amounts of time series data, such as we generated here using the LV model. Therefore, the usual data analysis relies solely on the inferred features. The data set for fitting parameters of the pairwise maximum entropy models is sampled across assembly sequences of a simulated data set. Prior to the sampling, we truncated the first 25 points of the sequences to remove the effect of initial conditions.

Murine gut microbiota - We applied our approach to the data of gut-microbiota taken from the feces of six male C57BL/6J mice, which are in the DDBJ database (http://trace.ddbj.nig.ac.jp/DRASearch/) under accession number DRA004786 (Nakanishi et al. submitted). Feces were sampled once every 4 weeks between 4 to 72 weeks of age, thus 18 data points were obtained per mouse. Hence, 96 data points are available. We transformed the relative abundance data into presence/absence data by setting a cutoff level as 1%, and we picked up OTUs that found between 20% to 80% samples. As the result, we obtained the presence/absence status of 8 OTUs specified at the genus level. We also used age of mouse (4-72 weeks) as an explicit environmental parameter. In the analysis, we scaled 4-72 weeks to a value within a 0-1 range. We assumed that 4-week interval was sufficiently longer than the transient dynamics of the gut microbiota (Gerber 2014), and treated microbiota composition of the same mouse at different ages as independent data.

Software

We used Mathematica (version 10.2, Wolfram Research, Inc., Champaign, Illinois, USA) to implement the method and generate simulation data. Computer codes (Mathematica notebook and package file) are available as online supporting information.

Results

Analysis of a competitive Lotka-Volterra system

As a demonstration, we analyzed the stability landscape of a 16-species competitive LV system with a fixed environmental condition ($\epsilon = 0$) having three stable states (Fig 3; see Appendix A for the parameter values). We first generated the simulated data set, calculated the features of a stability landscape, and sampled 256 compositions across assembly sequences to fit the parameters of the pairwise maximum entropy model. At the population level, there were sequences of extinctions and invasions, and the system finally converged to a stable state that was not invaded further. Below, in order to emphasize that we are considering community compositions, we denote a community composition as C_k instead of $\sigma^{(k)}$; k is an integer obtained by transforming a binary vector into a decimal number, e.g., if the community composition is (0,1,1,0,1), it is represented as C_{13}.

The stable states were C_{25233}, C_{38092} and C_{59852} and they appeared 5,332, 6,002, and 8,666 times within 20,000 simulations. We found 19,190 unique community compositions in the simulation out of $2^{16} = 65{,}536$ possible compositions. The length of the assembly sequences was 80 points and we used 75 points after truncating the first 5 points. Thus, we had $20{,}000 \times 75 = 150{,}000$ data points for calculating the features of the stability landscape. We focused on 1628 community compositions that appeared at least more than 20 times. While they are only 8% of the unique community compositions found in the assembly sequences, they covered 75% of observations, *i.e.*, a small fraction of community compositions appeared repeatedly.

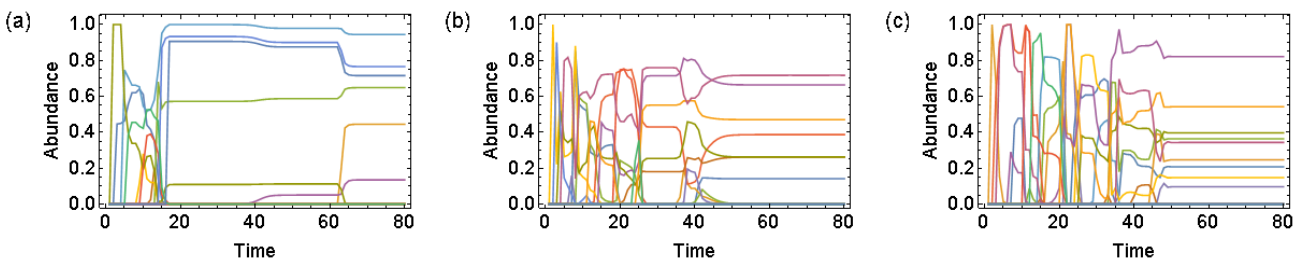

Figure 3. Examples of population dynamics that converged to three different stable states. (a) C_{25233}, (b) C_{38092} and (c) C_{59852}. See table 1 for the detail of community compositions.

Stable states	Composition	Number of observations	Attractive basin (precision)	Attractive basin (recall)
C_{25233}	(0,1,1,0,0,0,1,0,1,0,0,1,0,0,0,1)	5332	0.72	0.96
C_{38092}	(1,0,0,1,0,1,0,0,1,1,0,0,1,1,0,0)	6002	0.78	0.86
C_{59852}	(1,1,1,0,1,0,0,1,1,1,0,0,1,1,0,0)	8666	0.89	0.70

Table 1. Predictability of stable states.

Energy landscape of the LV system - Figure 4a shows the disconnectivity graph obtained from the energy landscape analysis of the LV system. Since we do not consider environmental variation in this case, we used eq. (4) for the analysis. The stable states identified by the energy landscape analysis were in perfect agreement with that of the LV system. Figure 4b is a scatterplot comparing the expected probability $P(\sigma^{(k)})$ calculated by the pairwise maximum entropy model (x-axis) and the empirical probability $\widehat{P}(\sigma^{(k)})$ (y-axis). This analysis is not specific to the energy landscape analysis but is a general criterion to assess the performance of maximum entropy models (Azaele et al. 2010). The Spearman rank correlation coefficient was 0.40 ($p<0.001$). This value shows the overall performance of the maximum entropy model to predict the occurrence of community compositions. However, this value may be underestimated because the number of observations is not large enough to make an accurate calculation for $\widehat{P}(\sigma)$ of rare community compositions. Figure 4c shows the relationship between the rescaled energy ($\overline{E}_k$) and relative convergence time (RCT; y-axis). The Spearman rank correlation coefficient was 0.36 ($p<0.001$), 0.69 ($p<0.001$), and 0.52 ($p<0.001$) for predicted attractive basins of C_{25233}, C_{38092} and C_{59852} and their weighted mean according to the number of observations (Table 1) was 0.55 ($p<0.001$). The correlation found here indicates that the energy landscape agrees well with that of the actual stability landscape, in the sense that it will predict the order in which community compositions appear during transient to stable states.

We next evaluate how well the energy landscape predicted the attractive basin. The color of each circle in figure 4c represents the attractive basin of the energy landscape. A filled or open circle represents whether it agrees (or disagrees) with the stability landscape. The overall result for the prediction is summarized as a confusion matrix

with both number of community compositions and observations (Fig. 4d). As suggested from the disconnectivity graph (Fig. 4a), the attractive basin of C_{38092} and C_{59852} are more easily mislabled with each other than those of C_{25233} and C_{38092} or C_{25233} and C_{59852}. To evaluate the predictive performance in more detail, we calculated precision and recall for different positions in the energy landscape according to the number of correct/incorrect observations (Fig. 4e-h). The overall precision and recall for the attractive basin of C_{25233}, C_{38092} and C_{59852} is in Table 1. The weighted mean of the precision and recall according to the number of observations of each stable state was 0.80 and 0.79, respectively. As the overall trend, both precision and recall increased when $\overline{E}_k$ decreased (Fig. 4e,f). Since community compositions having lower $\overline{E}_k$ are expected to be close to the stable states, this result suggests that the energy landscape is a good approximation of the stability landscape especially around the stable states. Furthermore, in addition to figure 4d, we see how the hierarchical relationship among the stable states (fig. 4a) reflect the relationship of stable states in the stability landscape. As energy decreased, the recall for the attractive basin of C_{25233} increases faster than that of C_{38092} and C_{59852} (fig. 4f). Moreover, the imbalance score (IS) for C_{25233} and (C_{38092}, C_{59852}) (here, C_{59852} is identified with C_{38092}) was always larger than that of C_{38092} and C_{59852} (fig. 4i). This suggest that the transition towards C_{25233} tends to be determined at an earlier stage of assembly processes compared C_{38092} and C_{59852}. In other words, these two community compositions are in close proximity in the stability landscape.

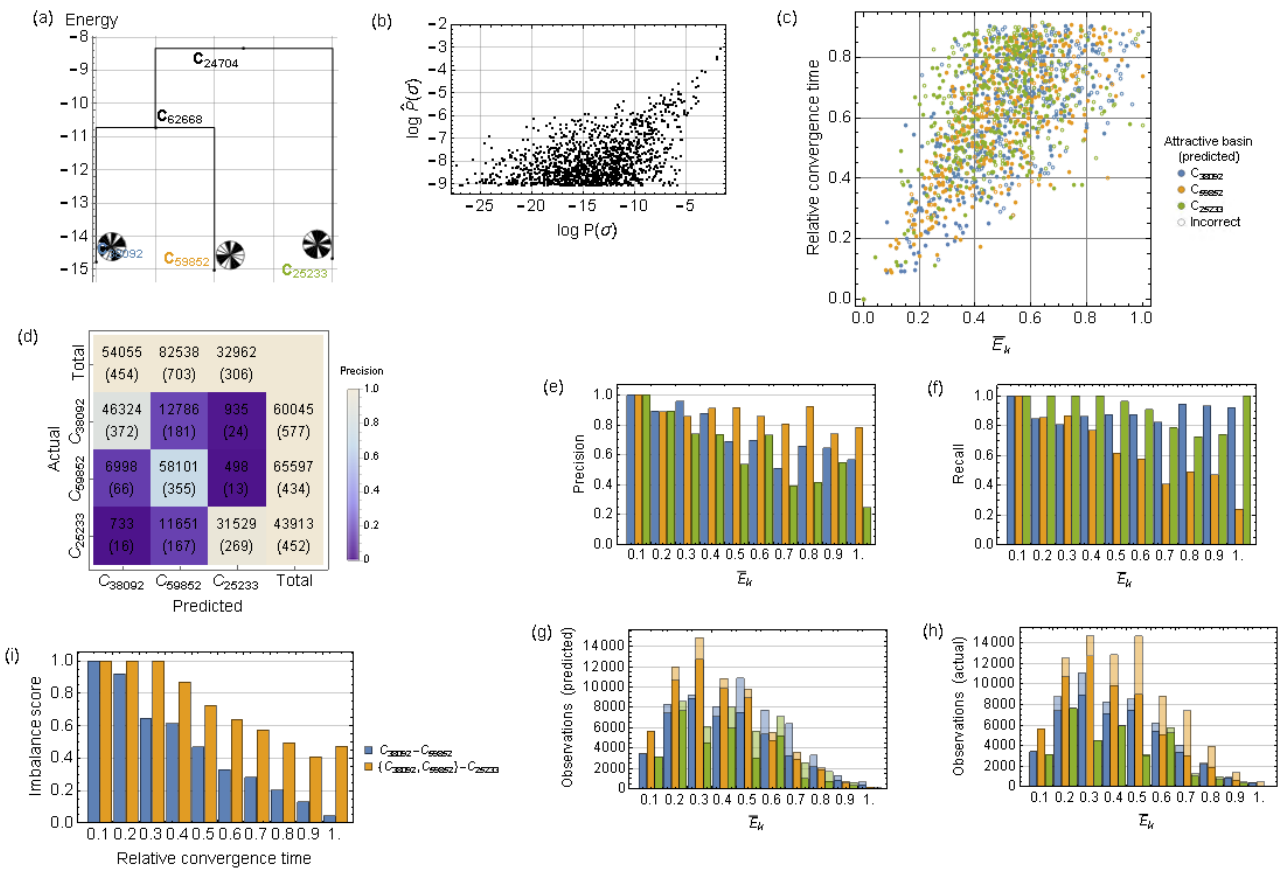

Figure 4. Energy landscape of a competitive LV system. (a) disconnectivity graph with three stable states and two tipping points. (b) scatterplot of the expected ($P(\sigma^{(k)})$) and empirical ($\hat{P}(\sigma^{(k)})$) probability for community compositions. (c) scatterplot of the rescaled energy ($\bar{E}_k$) and RCI for community compositions. The color of each circles represents the attractive basin of the energy landscape and filled or open circles indicate whether it agrees (or disagrees) with that of the stability landscape. (d) confusion matrix with the number of observations (the number of community composition is shown in parentheses). Here, observations of stable states were removed from the result. (e) precision of the prediction of attractive basin with respect to observations. (f) recall of the prediction on attractive basin with respect to observations. (g) total number of observations for predicted attractive basin. (h) total number of observations for actual attractive basin. In (e-h), values were calculated for $\bar{E}_k$ value grouped into 10 bins of equal width. Color of bars indicate predicted attractive basins in (g), and actual attractive basins in (h). Shaded area in (g, h) indicates observations with mismatch between actual and predicted attractive basin. (i) imbalance score calculated for the balance between C_{38092} and C_{59852} and C_{25233} and C_{38092}-C_{59852}. In the latter case, C_{59852} identified with C_{38092}.

Emulating community assembly dynamics - We consider the transition between stable states in the energy landscape to see how they inform about the ridge structure that lies between the basins of stability landscape. Since we are considering assembly dynamics starting from an empty state, such ridge states may correspond to a set of community compositions where the terminal stable state is almost unique below it (i.e., they may be representing the points of no return in assembly processes). If a community composition is located on a ridge, it will have an intermediate RCT value in the sense that it is apart from both the stable states (where RCT is 0) and the states at the earlier stage of assembly dynamics (where RCT is close to 1). Also, because the dynamics are less deterministic on the ridge, it's IS will be lower than that of other community compositions having a comparable energy.

Here, to demonstrate how we can use the dynamics of energy landscape to study the ridge structure, we investigated the transitions between the stable state C_{38092} and C_{59852} in more detail. By using the heat bath algorithm, we collected 5,000 transition sequences of community compositions from C_{38092} to C_{59852} (C_{59852} to C_{3809}). We then extracted the community composition having the highest energy in each transition sequence as the effective boundary between them. There were 1,616 such compositions and, as shown in Figure 5a, in the LV simulation, 81% of 14,668 sequences that converged to C_{38092} or C_{59852} (Table 1) contained one of these compositions. When we focusing on the top 100 low energy compositions (shortly, we call them *channels*), 56 among them (0.3%, that is 53 out of 19,190, of all observed community compositions) actually appeared in 52% (7596 out of 14,668) of LV sequences. Figure 5b is the scatterplot showing the energy and RCT of community compositions where channels are highlighted as red points, and Figure 5c is the smoothed histogram of the RCT of channels and that of all community compositions. RCT of channels had a median of 0.33, which was significantly ($p<0.001$) lower than that of all compositions which was 0.65. Furthermore, IQR (difference between the third and first quartiles) of channels was 0.16 and it was significantly ($p<0.001$) lower than that of all compositions which was 0.29. Thus, channels tended to be clustered in a narrow area of the lower part of the stability landscape. Figure 5d shows RCT and IS of channels (red) or other 130 community compositions in the range of energy where channels are distributed (Fig. 5b). The median of IS was 0.60 for channels and it was significantly ($p<0.01$) smaller than that of others which was 0.70. From the above, it can be said that there is a certain relationship between the ridge that controls the transitions between C_{38092} and C_{59852} on the energy landscape and the structure of the stability landscape that determines direction of assembly towards C_{38092} or C_{59852}.

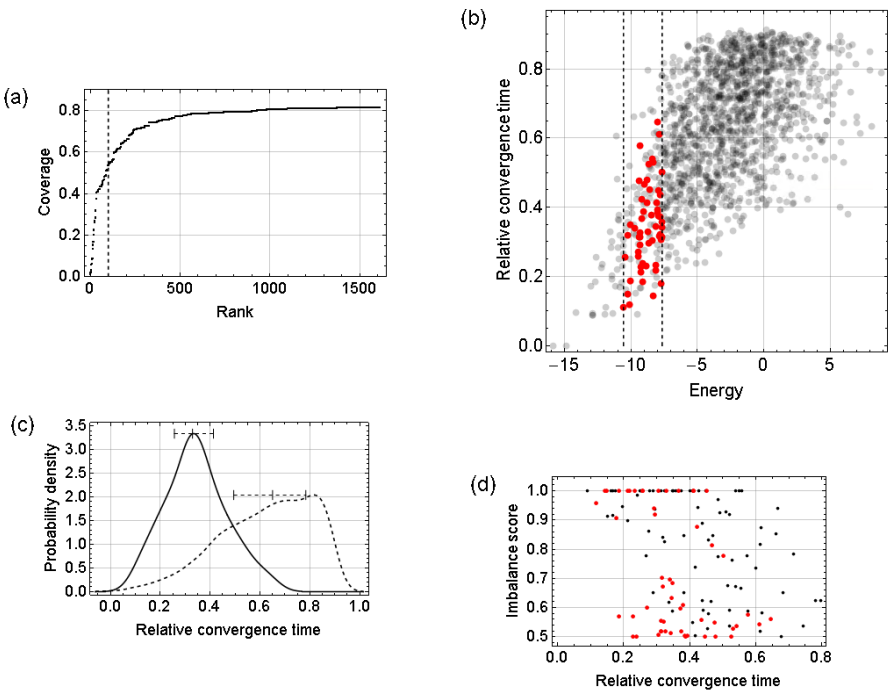

Figure 5. Emulated compositional dynamics between stable state C_{38092} and C_{59852}. (a) coverage of assembly sequences of the simulated data set that converged to C_{38092} or C_{59852} (14,668 in total) including the community compositions in effective boundary ranked by their energy. Dashed line indicates top 100 community compositions (channels). (b) smoothed histogram of RCT of channels and that of all community compositions. (c) scatterplot with energy and RCT for community compositions belonging to the attractive basin of C_{38092} and C_{59852}, where channels are indicated by red points. (d) relationship between RCT and IS, where channels are indicated by red points.

Energy landscape across environmental gradient - If the occurrence of species depends on some abiotic factors, change in the stability landscape in response to environmental changes will be observed. Here, we generated simulated data sets with variation in environmental parameter ϵ and a fixed response vector b (see Appendix A for the parameter values), and demonstrate how the energy landscape of the extended pairwise maximum entropy model can capture the change in the stability landscape across ϵ.

We generated a simulated data set for ϵ at every 0.01 steps between 0 and 1 to calculate the features of a stability landscape. Figure 6a shows how the number and composition of stable states changes with respect to ϵ. The black lines show the range of ϵ in which a community composition was observed as a stable state. There were

three branches that originated from C_{59852}, C_{25233} and C_{38092}; C_{59852} disappeared at $\varepsilon = 0.08$, C_{25233} changed to C_{58001} at $\epsilon = 0.125$ and then disappeared at $\varepsilon = 0.3$, and C_{38092} sequentially changed to five other community compositions across $\epsilon = 0$ to 1.

We randomly sampled 256 community compositions from the above data set for the parameter fitting of the extended pairwise maximum entropy model and then applied the energy landscape analysis. Our approach identified all existing branches of stable states and slightly over-estimated the range of ϵ in which they exist (Fig. 6b). Also, it well captured the sequence of the transition of community compositions within the branch of C_{25233} and C_{38092} except for false detection of C_{41617} and non-detection of C_{38284}. The correlation between $\hat{P}(\sigma)$ and $P(\sigma)$ (Fig. 6c) was around 0.4 and slightly decreased with ϵ. This value was comparable to the corresponding value in the constant environment we described above (0.40). Correlation between RCT and $\bar{E}_k$ (Fig. 6d) was not largely different before $\epsilon < 0.6$, most different above 0.4, and then it started to decrease. While we did not investigate the reason in detail, this might be due to the increase of the stability of a single stable state that can reduce the variety of community compositions other than the stable state within the data set. Overall, however, the addition of an environmental axis did not significantly reduce the accuracy of the stability landscape estimates.

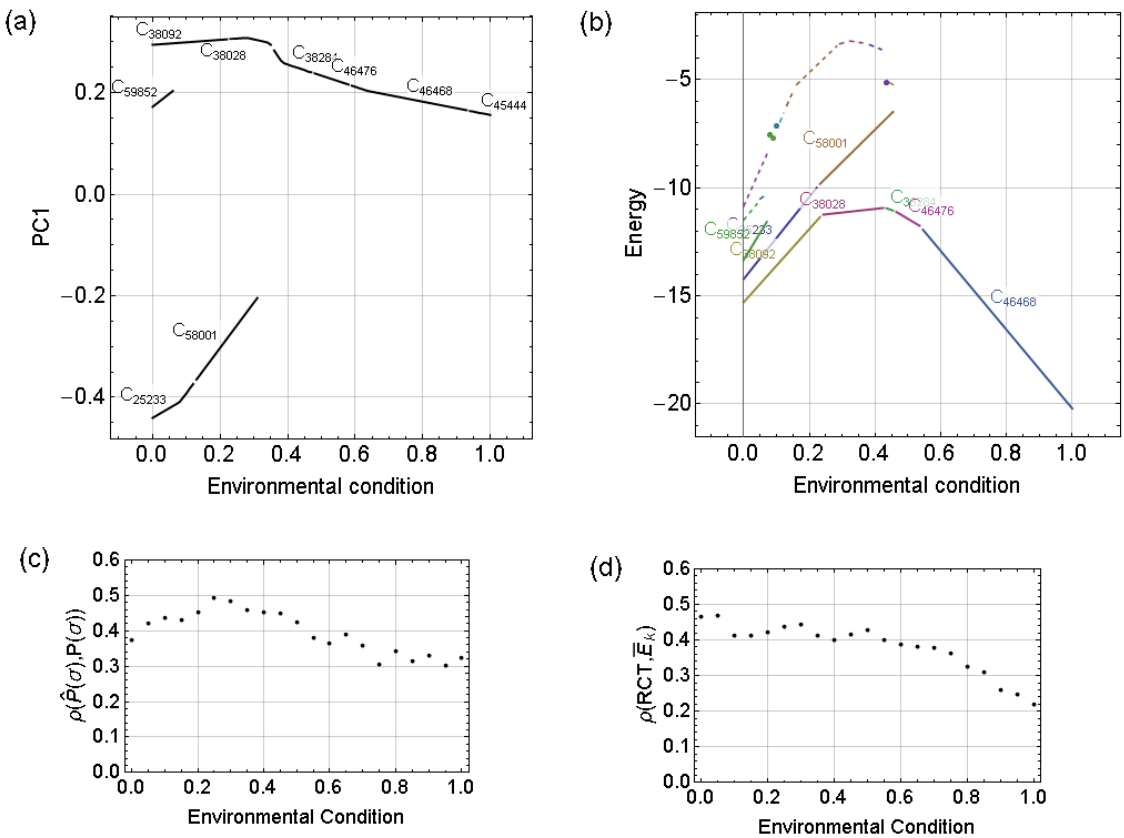

Figure 6. Change of stability landscape and energy landscape in response to environmental change. (a) stable state diagram calculated from simulated data sets. Here, vertical axis is PC1 calculated from PCA including all stable states. (b) stable state diagram obtained from the energy landscape analysis. Solid lines indicate stable states and dashed lines indicates tipping points. (c) Spearman rank correlation between the expected ($P(\sigma^{(k)})$) and empirical ($\hat{P}(\sigma^{(k)})$) probability for community compositions. (d) Spearman rank correlation between the rescaled energy ($\bar{E}_k$) and RCI for community compositions.

Benchmarking

In our baseline condition (A in Fig. 7), the median of Spearman rank correlation between empirical and expected probability for the community compositions was 0.43, for RCT and $\bar{E}_k$ the same value was 0.51. The median of both precision and recall was 1 for stable states, and 0.79 for attractive basin. Reducing the number of stable states in the LV system only modestly affected the results (B in Fig. 7), but increasing it slightly made it difficult to predict attractive basins (C in Fig. 7). This is unsurprising given that it increases the likelihood of confusion among basins. Increasing the number of species tended to make identification of stable states and attractive basins more difficult (D in Fig. 7). However, the difference would be small, given that the total number of possible compositions of 24 species system is 256 times larger than 16 species model. Although increase of data set size had improved the results when comparing 128 and 512 data point cases (E and F in Fig. 7), no improvement was found when comparing 256 and 512 data point cases (A and F in Fig. 7). Because of the fundamental difference between the stability landscape and the energy landscape, this would indicate the limitations of approximating the former by the later. Both Type II functional response (G) and system noise (H) were not largely altered the results, but slightly reduced the correlation between $\bar{E}_k$ and RCT.

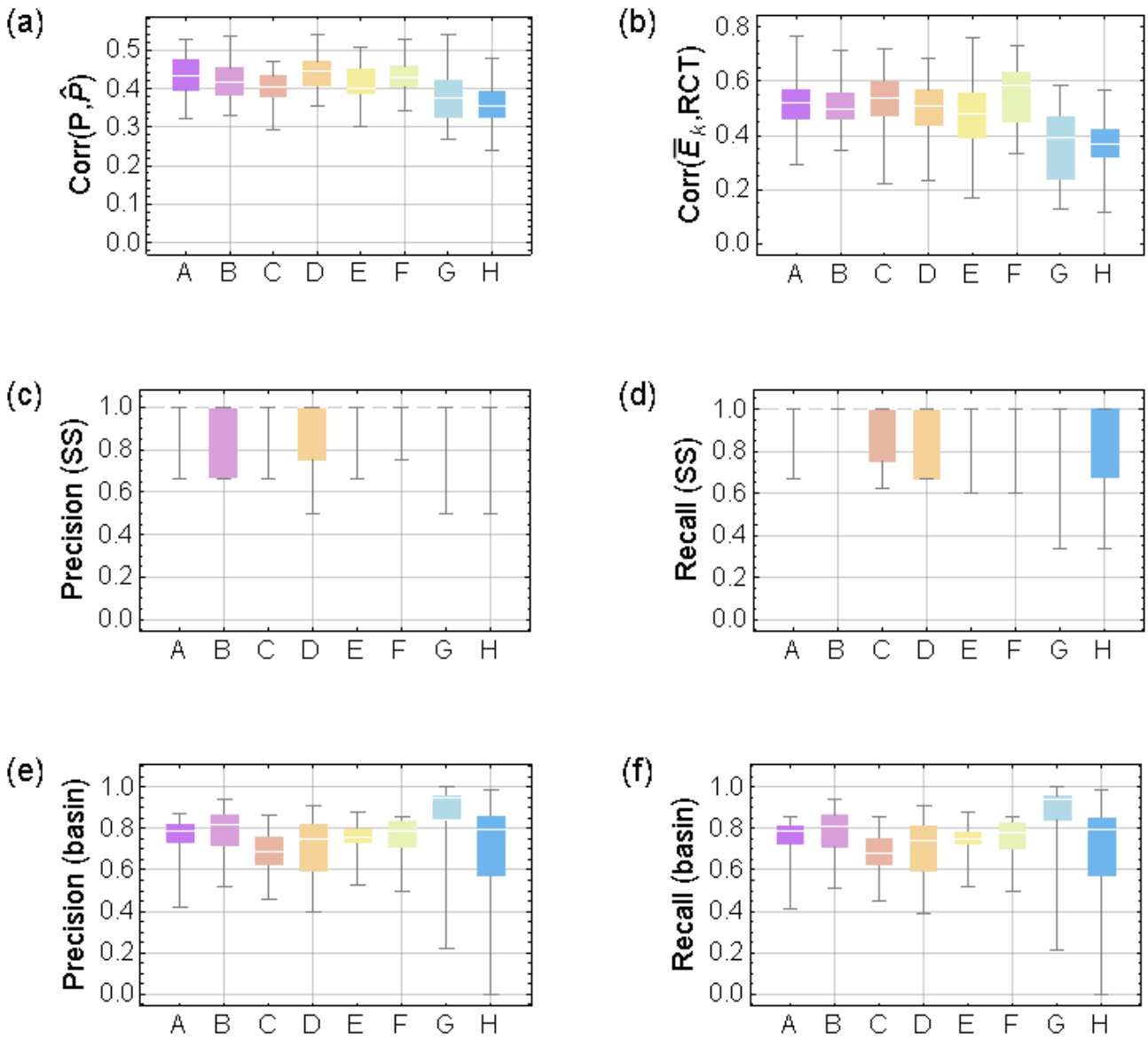

Figure 7. Benchmarking with different simulation conditions. Spearman rank correlation between (a) expected and empirical probability for community compositions, and (b) rescaled energy and RCT, (c, d) precision and recall for the prediction on stable states and (e, f) the same values for attractive basin. Precision (recall) for stable states is calculated by the ratio of correctly identified states in the predicted (actual) stable states, and the same values for attractive basin are weighted by the number of observations (see main text). The median and the first and third quartile value was 1 in A,C,E,F, G, H in (c) and A,B,E,F, C in (d). In B, D in (c) and C, D, H in (d) the median and the third quartile value was 1. We used 30 independent datasets for each simulation condition. Summarizing the simulation conditions as (number of species, number of stable states in LV system, number of samples, type of functional response, strength of noise), they are, A: (16, 2, 256, 1, 0), B: (16, 2, 256, 1, 0), C: (16, 4, 256, 1, 0), D: (24, 3, 256, 1, 0), E: (16, 3, 128, 1, 0), F: (16, 3, 512, 1, 0) , G: (16, 3, 256, 2, 0) , H: (16,

3, 256, 1, 0.1). Here, for the type of functional response, 1 indicates Type I and 2 indicates type II. See Appendix A for more information.

Application to real data

We applied our approach to the gut microbiome data of six mice with 96 samples. Community compositions were represented by eight genus level OTUs that can be identified as species in the above analysis, and we used age of mice as the environmental condition (i.e., only one environmental factor was considered). Since we included only age as the environmental factor in the analysis, in the extended pairwise maximum entropy model (eq. (2)), ε is a scalar associated with each sample and g is a vector that represents response of each species to age.

At the community level, there were two stable states C_{227} and C_{93} at initial age (Fig. 6a). C_{227} remained until 72 weeks and showed reduced energy with increasing age. C_{93} had lower energy than C_{227}, and increased energy as age increased. C_{93} changed to C_{125} at 29 weeks of age and then showed reduced energy with increasing age. C_{125} further changed to C_{253} at 38 weeks of age. The energy of C_{125} and C_{253} was lower than C_{227} up to 72 weeks of age. The difference in the height of the energy barriers between the two alternative stable sates (i.e., distance between the stable states to the tipping point with respect to y-axis in Fig. 8a) decreased with increasing age until C_{125} changed to C_{253}. These results suggest that C_{93} is more representative of gut microbiota during early life stages. The difference between C_{93} and C_{227} was the presence of a group of three genera (unclassified Lachinospiraceae, unclassified Ruminococcaceae and *Oscillospira*) or *Sutterella* (Table 2). Although C_{93} did not contain *Turicibacter* and *Bifidobacterium*, these genera sequentially appeared as C_{93} changed to C_{253}: *Turicibacter* appeared when C_{93} changed to C_{125} and *Bifidobacterium* appeared when C_{125} changed to C_{253}.

In addition to the height of energy barriers, the number of community compositions and energy distribution of the attractive basins provides information on the robustness and variability of stable states. Figure 8b shows the energy distribution of community compositions in the attractive basins of C_{93} and C_{227} at 10 weeks of age. The median and IQR of the two energy distributions were almost the same, but the difference in the number of community compositions was large (Fig. 8b, Table 2). In other words, C_{93} is more stable to stochastic variation than C_{227} in the sense that it has a larger attractive basin. However, this difference almost disappeared by 60 weeks of age (Fig. 8c, Table 2). On the other hand, the difference between the median and stable state energies was

6.76 for C_{93} and 3.87 for C_{227} in 10 weeks of age (Table 2). This was mainly because of the fact that C_{93} had a sharp decline in energy around the stable state (Fig. 8d), which is also indicated by the smaller kurtosis for C93 than C227 (Table 2). Interestingly, in C253, which is on a branch of C93 (Fig. 8a), the difference between the median and stable state energies was decreased (accompanying the increase in kurtosis) (Fig. 8c, Table 2) despite the decrease in stable state energy. This resulted in a reduced slope around the stable state (Fig. 8e), and lead to increase in the amplitude and autocorrelation of compositional variation around C_{253} (Fig. 8f, g).

This is not specific to energy landscape analysis, but analysis on the estimated parameters provide some insights into the mechanisms behind community level responses (Azaele et al. 2010, Harris 2016). In figure 9a, the community level response is shown by the bars marked as 'Total' in addition to the genus level responses. The net effect of interspecific relationships ($\Sigma_j J_{ij} \sigma_i^{(k)} \sigma_j^{(k)}$), the bacterial responses to age ($g_i \epsilon$), and the implicit effect of environmental factors (h_i; here, these values represent the sum of the effects other than the bacterial response to age or the biotic interaction between bacteria) are indicated by blue, orange and green, respectively. There were positive relationships among Lachinospiraceae, Ruminococcaceae and *Oscillospira* (Fig. 9b) and these relationships made up most of the interspecific relationships in C_{93}, C_{125} and C_{253} (Fig. 9a). The three genera had a negative relationship with *Suterella* (Fig. 9b). Thus, they could be mutually exclusive, which was responsible for the presence of two alternative stable states over age. *Sutterella* had a positive relationship with *Turicibacter* and *Bifidobacterium*, supporting their presence in C_{227} (Fig. 9). In contrast, *Turicibacter* and *Bifidobacterium* had a negative relationship with Lachinospiraceae, Ruminococcaceae and *Oscillospira*. Thus, they were absent from C_{93} and then appeared as an effect of age. The correlation between age and the occurrence of a genus became positive if g (genus level response to age; Table 3) was positive; this correlation became negative when g was negative. The sum of g across community members determined the community level response to age (Fig. 8a). Since both *Turicibacter* and *Bifidobacterium* were positively affected by age, they appeared with increasing age despite their negative relationship with Lachinospiraceae, Ruminococcaceae and *Oscillospira*. In Fig. 9a the effect of interspecific relationships with *Turicibacter* in C_{125} was negative while it was positive in C_{253} because of a positive relationship with *Bifidobacterium* (Fig 9b). The relationship between *Turicibacter* and *Bifidobacterium* also facilitated the appearance of *Bifidobacterium* at 38 weeks of age (Fig. 8a). Because of their positive relationship with age, the appearance of *Turicibacter*

and *Bifidobacterium* changed the community level response to age when C_{93} changed to C_{125} and C_{125} changed to C_{253}.

Our result showed that there were two alternative stable states and their relative stability (difference in the height of the energy barriers between them) changed over age. To examine how this result explains microbial population dynamics represented by relative abundance data, we applied analysis of similarity (ANOSIM) to abundance of the 8 genera used for the energy landscape analysis. ANOSIM statistics of the abundance data grouped with age (4-28 or 48-72 weeks) across different individuals was -884.8 ($p<0.001$), suggesting a difference in gut microbiota among early and later life stages. We then grouped abundance data with individuals in 4-28 or 48-72 weeks and applied the same analysis. ANOSIM statistics were -65.2 ($p<0.001$) for 4-28 weeks and -37.6 ($p=0.097$) for 48-72 weeks. Thus, individual dependency of microbiota was strong in the early life stage and weakened in the later life stage. This was in correspondence with the structure of the energy landscape at 4-28 weeks; since the energy barrier was higher and attractive basin is larger for C_{93} than C_{227} (Fig. 8a, b), community composition would more likely remain in the basin of C_{93} once it shifted from that of C_{227}. At 48-72 weeks, switching between C_{227} and C_{253} is more likely because of the increased autocorrelation and amplitude of compositional variation (Fig. 8g) as well as the small difference in energy barrier between the two stable states (Fig. 8a), and it would reduce the individual dependency of stable states.

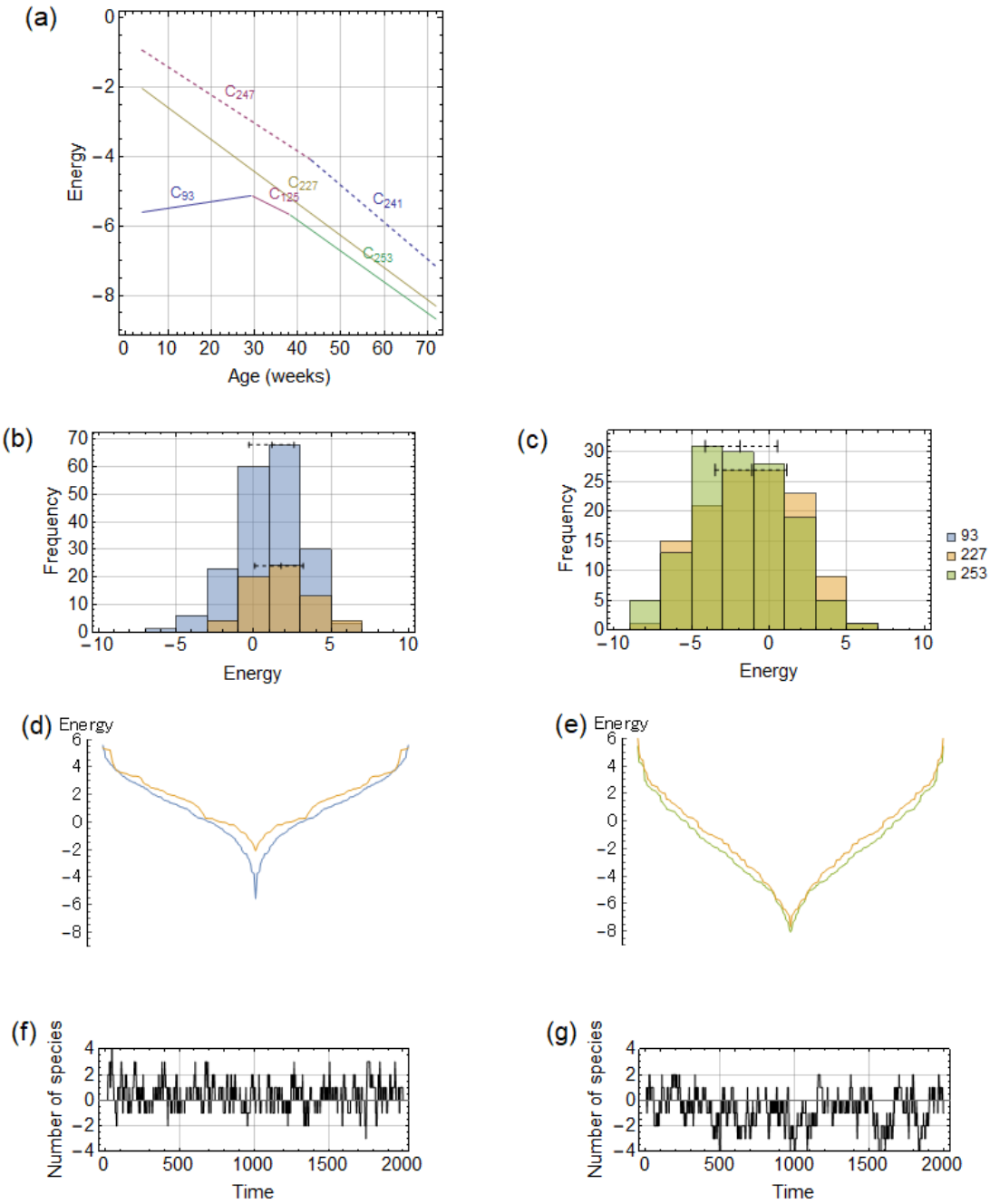

Figure 8. Stability of a murine gut microbiota. (a) stable state diagram showing the energy of stable states and tipping points. Here, both stable states (solid lines) and tipping points (dashed lines) are shown. Each line segment labeled by community composition represents the range of age in which stable states (or tipping points) exist. (b) the energy distribution of community compositions in the attractive basins of C_{93} and C_{227} at 10 weeks of age. (c) the energy distribution of community compositions in the attractive basins of C_{227} and C_{253} at 60 weeks of age. In (b, c) horizontal bars indicate the median and IQR. (d) slope of the attractive basin of C_{93} (blue) and C_{227} (yellow) in 10 weeks of age. (e) slope of the attractive basin of C_{227} (green) and C_{253} (yellow) in 60 weeks of age. (f) emulated compositional dynamics around C_{253}. (g)

emulated compositional dynamics around C_{253}. In (f, g) vertical axis shows the number of species of corresponding time point minus that of the stable state.

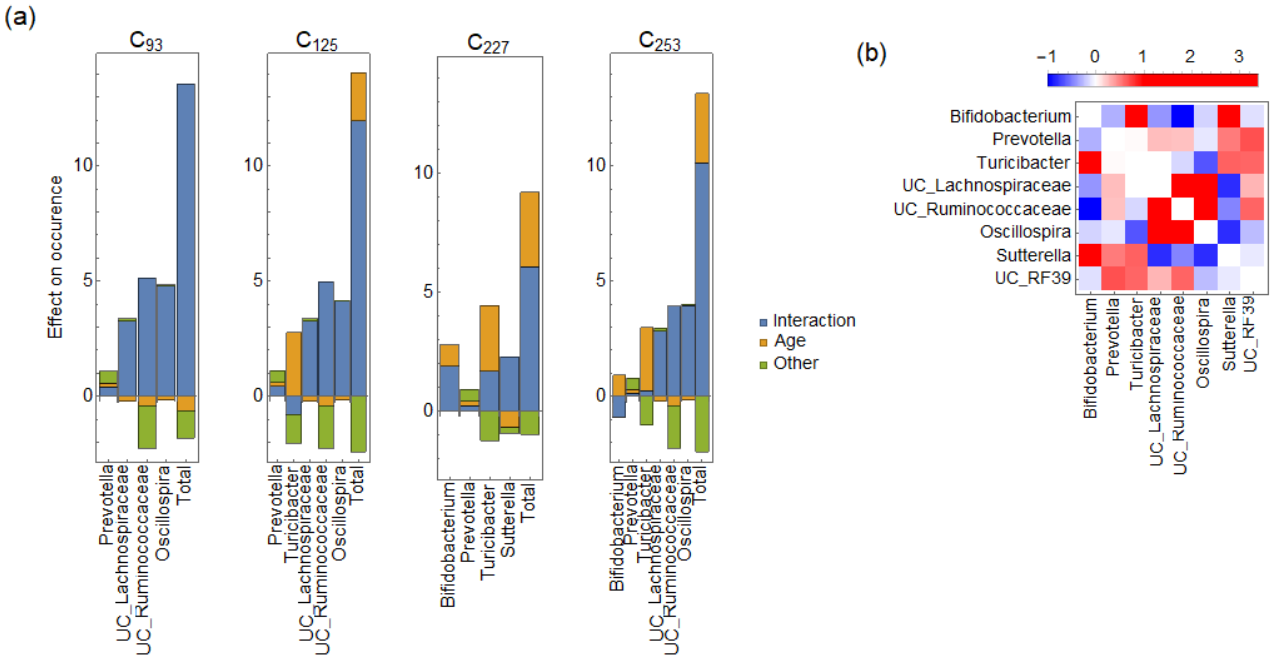

Figure 9. Estimated parameters for a murine gut microbiota. (a) Strength of the net effect of interspecific relationship ($\Sigma_j J_{ij}\sigma_i^{(k)}\sigma_j^{(k)}$), observed environmental factor (response to age) ($g_i\varepsilon$) and unobserved environmental factors (h_i) for each genus i (genus level effects) and their sum over community members (community level effects), $\Sigma_i\Sigma_j J_{ij}\sigma_i^{(k)}\sigma_j^{(k)}$, $\Sigma_i g_i \epsilon \sigma_i^{(k)}$ and $\Sigma_i h_i \sigma_i^{(k)}$ (shown as 'total'). $\sigma_i^{(k)}$ represents membership of each communitie (Table 3). For comparison, we set $\epsilon = 0.5$. (b) elements of biotic interactions (J_{ij}). The value represents the strength of association between two genera (shown in columns and rows). There is a positive association between two genera if the value is positive whereas there is negative association if it is negative.

	10 weeks						60 weeks					

	Number of community compositions	Median	Min (stable state)	Median-Min	IQR	Kurtosis	Number of community compositions	Median	Min (stable state)	Median-Min	IQR	Kurtosis
C_{93}	191	1.16	-5.59	6.76	2.90	2.90	0	n/a	n/a	n/a	n/a	n/a
C_{227}	65	1.77	-2.10	3.87	3.12	2.28	124	-1.11	-7.68	6.58	4.62	2.29
C_{253}	0	n/a	n/a	n/a	n/a	n/a	132	-1.87	-8.08	6.21	4.66	2.34

Table 2. Summary statistics of the energy distribution of attractive basins.

	h	g	C_{93}	C_{125}	C_{227}	C_{253}	C_{241}*	C_{247}*
Bifidobacterium	-0.003	1.814	0	0	1	1	1	1
Prevotella	0.509	0.337	1	1	1	1	1	1
Turicibacter	-1.246	5.512	0	1	1	1	1	1
UC_Lachnospiraceae	0.114	-0.458	1	1	0	1	1	1
UC_Ruminococcaceae	-1.84	-0.844	1	1	0	1	0	0
Oscillospira	0.038	-0.318	1	1	0	1	0	1
Sutterella	-0.249	-1.395	0	0	1	0	0	1
UC_RF39	-3.203	1.321	0	0	0	0	0	0

Table 3. Profile of eight genera included in the analysis. h (effect from unobserved environmental factors) and g (genus level response to age) are the parameters inferred by stochastic approximation, and 0/1 values indicate membership of each genus in stable states and tipping points (marked by *).

Discussion

We developed a framework to study stability landscapes that govern the compositional dynamics of multispecies communities by incorporating pairwise maximum entropy models (Azaele et al. 2010, Araujo et al. 2011, Harris 2016, Clark et al. 2018) and the energy landscape analysis (Becker and Karplus 1997, Wales et al. 1998, Watanabe et al. 2014). We showed that, with a relatively small amount of data, our method is able to identify the features characterizing the stability landscape, i.e., it successfully detects stable states (Table. 1) and predicts attractive basin (Fig. 4e-h), the position of each community composition with respect to the stable states (Fig.4c), and whether a

community composition is on a ridge of attractive basins in which end state is not uniquely determined (Fig.4i, Fig5). It was confirmed from multiple different data sets that these results were mostly robust to different simulation conditions (Fig. 7), although the results suggested the limitation of approximating the stability landscape as the energy landscape. Some sophistication of the model fitting framework including sparse modelling would be required to improve the performance. We also demonstrated that the same analysis was applicable to the case in which environmental conditions for each sample was different (Fig.6), without the need for increasing the amount of data. This result highlights that our method reliably captures the change of the overall compositional stability of a multispecies community over environmental change, which we regarded as the requisites for integration of compositional stability and regime shift concepts.

There will be several ways to further pursue this direction. For example, development of the early warning signals (Scheffer et al. 2012, 2015) for shifts of stable states in empirical multispecies communities is worth investigating further. Our analysis suggested that a small fraction of community compositions may be a channel for transition between alternative stable states (Fig. 5). If a system is in one of such states, it may indicate increasing probability of transition to other stable states. This would be a basis for developing an early warning signal and considering some possible intervention to prevent such shifts. Secondly, given how spatial scale interacts with the drivers of community assembly (e.g. Chase 2014), the results of energy landscape analysis should be interpreted in light of the spatial scale of total sampling extent to disentangle the drivers of community assembly across scales (Viana & Chase 2019, Ross et al. submitted). If the spatial extent of observations is large and the effect of environmental heterogeneity is significant, by choosing a relevant environmental factor (or appropriately reducing multiple factors into a single dimension), the shift of stable community compositions can be unfolded with respect to the parameter as in the stable state diagram (Fig. 6b). One could then explore whether the model's explanation is consistent with our process-based understanding of community assembly dynamics. Such an approach would complement existing methods proposed to assess the relative importance of the ecological processes that drive community assembly (Legendre et al. 2009, Meynard et al. 2013, D'Amen et al. 2018, Mertes & Jetz 2018).

In the mouse gut microbiota, our approach showed the presence of two alternative states over age (Fig. 8a). The difference between the two stable states was characterized by presence of *Suterella* or unclassified Lachinospiraceae, unclassified Ruminococcaceae and *Oscillospira* (Table 3). Our result suggested that the stable state

containing the three genera (C_{93}) was more representative of the gut microbiota during early life stages because it had lower energy than the counterpart (C_{227}) and became relatively unstable with increasing age (Fig. 8f, g). Langille et al (2014) reported that Lachinospiraceae, Ruminococcaceae and *Oscillospiraceae* are phylogenetically closely related and characterize the mouse gut microbiota during early life stage. This result supports tight associations among these groups and their role of characterizing a stable state representing early-life gut microbiota. C_{93} changed to C_{125} (29 weeks age) and C_{125} changed to C_{253} (38 weeks age) due to appearance of *Turisibacter* and *Bifidobacterium*, respectively. The response of *Turicibacter* and *Bifidobacterium* to age had a prominent role in the community level response during these shifts. However, the importance of interspecific relationships was also identified. Since *Turicibacter* and *Bifidobacterium* had a negative relationship with Lachinospiraceae, Ruminococcaceae and *Oscillospira*, they could not appear until 28 and 39 weeks of age, respectively. Here, presence of *Turicibacter* facilitated appearance of *Bifidobacterium* due to their positive relationship. In terms of the height of energy barriers, the transition between alternative stable states tended to be unidirectional (from C_{227} to C_{93}) in the early life stage and bidirectional in the later life stage (between C_{227} and C_{125} or C_{253}). Furthermore, the mechanism of changing compositional variability was inferred from the analysis of energy distribution of attractive basins. Our results suggest that there were two mechanisms. The first is the change in the number of community compositions in the attractant basin, which directly affects the magnitude of compositional variability to which an attractive basin accommodates, and thus corresponds to Holling's ecological resilience (Holling 1996). The second is the change in the shape of attractive basin, especially related to the kind of curvature around the stable state (Fig. 8d, e). This relates to the return time to a stable state, and corresponds to Holling's engineering resilience (Holling 1996). Not only the change in the height of barrier between stable states but also these mechanisms governing compositional variability works synergistically in the age-related loss of stability in murine gut microbiota.

Compositional dynamics play a prominent role in real world ecosystem organization. Understanding community assembly in terms of the management of ecological systems has direct relevance to conservation biology, agriculture, and medicine (Fukami et al. 2015). Here, as an approximation of stability landscape, energy landscape would provide a reliable map for those who seek an effective path between different community compositions. In conservation biology, knowledge of the paths by which communities are assembled helps ecologists to understand the role of history in shaping current communities, and is important for effective community restoration

(Weiher and Keddy 1999, Lockwood & Samuels 2004, Suding et al. 2004, Wilsey et al. 2015, Young et al. 2005, 2015). In other words, when historical contingency occurs, restoring and maintaining native biodiversity may require specific sequences of exotic species removal and/or native species introduction. This is also relevant to agriculture, e.g., the successful inoculation of agricultural soils with beneficial fungi or other microbes may depend on the timing of inoculation relative to plant growth, as well as the profile of other soil microbes (Verbruggen et al. 2013, Toju et al. 2018). In medicine, the relevance of historical contingency in community assemblies to curing some human diseases is being recognized (Costello et al. 2012, Fierer et al. 2012, Lam & Monack 2014, Devevey et al. 2015). Clinically meaningful evidence for the potential application of modulating the intestinal microbiota for therapeutic gain has created considerable interest and enthusiasm (Smits et al. 2013, Li et al. 2016, Shetty et al. 2017). Other than *Clostridium difficile* Infection (CDI), a disruption to the gut microbiota is associated with, e.g., irritable bowel syndrome, autism, obesity, and cavernous cerebral malformations (Karczewski et al. 2014, Cox et al. 2015, Tang et al. 2017). Driving disrupted microbial communities back to their healthy states could offer novel solutions to prevent and treat complex human diseases.

There would be some alternative methodology to study stability landscapes. Dynamical models (such as differential equations) are able to describe shifts in community compositions based on the gradual changes in population abundance of species (Gravel et al. 2011). If we are able to estimate the parameters of a dynamical model, it allows us to directly study the stability landscape that is inferred from observational data. However, it is generally difficult to develop fully mechanistic models for multi-species communities. The complex nature of microbial interactions makes it difficult to formulate all the present relationships into mathematical formulations (Hartig and Dormann 2013; Perretti et al. 2013a, b; De Angelis and Yurek 2015). Moreover, a theoretical study proved that finding a precise dynamical equation for a time-series is, in general, computationally intractable even with any amount/quality of data (Cubitt et al. 2012). Another potential approach may be developing a Markov chain model with a transition matrix between different community compositions (Wootton 2001). This can be done if we can obtain multiple observations on two consecutive community compositions. However, considering the number of possible paths in a multispecies system, it might not be a realistic approach. Actually, in our LV model with a constant environment, among randomly sampled 128 pairs of consecutive community compositions (comparative to the 256 data points used to fit pairwise maximum entropy models), 88.1% (s.d. 3.8) of them were observed only once. Thus, it is obvious that it requires much more data to reconstruct a transition matrix. Recently developed

methods for reconstructing low dimensional potential landscape (Gibson et al. 2017, Shaw et al. 2019, Chang et al. 2019) would be an appealing option, but since this approach projects microbial dynamics onto a low dimensional potential landscape, it is unable to reproduce overall compositional stability as we see in this paper. Also, it is unable to track the change of compositional stability across environmental parameters. Considering the data set size and observational procedure required, our method can be considered as a realistic option to study compositional stability of empirical communities.

There are still some flaws that need to be addressed. Further verification is required to assess the effect of replacing species' abundance with presence/absence status. Does the pairwise maximum model always provide good approximation to the stability landscape? For example, since our approach relies on a gradient system, it cannot account for attractor dynamics that often appear in ecological systems. Heteroclinic cycles that cause cyclic alteration of community compositions (Morton and Law 1997, Fukami et al. 2015) are one example. These dynamics may still be identified as a set of stable states separated by low energy barriers, though the overall consequence of approximating dynamics in a continuous phase space into a coarse-grained phase space (where nodes of the weighted network represent each sub-system of the original phase space) is unknown. Also, causal relationships between species' presence/absence status and transition of one community state to another are not well represented using our approach. Incorporating causal analysis (e.g., Sugihara et al. 2012, Runge et al. 2017) will strengthen our approach especially when considering its application to control community states.

Conclusion

In this paper, we demonstrated the effectiveness of pairwise maximum entropy models as an approximation of overall compositional stability, which we defined as a stability landscape, of multispecies communities in a changing environment. The framework of energy landscape analysis played a prominent role for the success of this approach. Our model opens up new research directions encompassing the concept of alternative stability in community assemblies of multispecies communities and the change in dynamical stability across environmental changes, which have mainly been studied in low-dimensional systems in the past decades. There are urgent demands for a methodology that is able to account for compositional dynamics in multispecies communities. Although some further verification and improvement is required, we believe that the methodological advancement presented here will be a new systemic

paradigm for developing a predictive theory for real-world ecological communities (Long and Karel 2002, Chase 2003, Fukami 2010, Mouquet et al. 2015).

Acknowledgements

This work was supported by the Management Expenses Grant for RIKEN BioResource Research Center, MEXT, and in part by the Center of Innovation Program from Japan Science and Technology Agency (JST) (to K.S. and S.N.), JST PRESTO JPMJPR16E9 (to S.N.), JPMJPR1537 (to S.F.), the Japan Society for the Promotion of Science (JSPS) KAKENHI 20K06820 and 20H03010 (to K.S.), JP15H05707 (to S.N.), 18H04805 (to S.F.), AMED-CREST JP20gm1010009 (to S.F.), JST ERATO JPMJER1902 (to S.F.), the Takeda Science Foundation (to S.F.), the Food Science Institute Foundation (to S.F.) and the Program for the Advancement of Research in Core Projects under Keio University's Longevity Initiative (to S.F.). We declare that we have no conflict of interest.

References

1. Drake, J. A. (1991). Community-assembly mechanics and the structure of an experimental species ensemble. *The American Naturalist*, 137(1), 1-26.
2. Fukami, T., Morin, P. J. (2003). Productivity–biodiversity relationships depend on the history of community assembly. *Nature*, 424(6947), 423.
3. Fukami, T., Dickie, I. A., Paula Wilkie, J., Paulus, B. C., Park, D., Roberts, A., et al. (2010). Assembly history dictates ecosystem functioning: evidence from wood decomposer communities. *Ecology letters*, 13(6), 675-684.
4. Jiang, L., Joshi, H., Flakes, S. K., Jung, Y. (2011). Alternative community compositional and dynamical states: the dual consequences of assembly history. *Journal of Animal Ecology*, 80(3), 577-585.
5. Fukami, T. 2010. Community assembly dynamics in space. In Community ecology: Processes, models, and applications. Edited by Herman A. Verhoef and Peter J. Morin, 45–54. Oxford: Oxford Univ. Press.
6. Fukami, T. (2015). Historical contingency in community assembly: integrating niches, species pools, and priority effects. *Annual Review of Ecology, Evolution, and Systematics*, 46, 1-23.
7. Schröder, A., Persson, L., De Roos, A. M. (2005). Direct experimental evidence for alternative stable states: a review. *Oikos*, 110(1), 3-19.
8. Pu, Z., Jiang, L. (2015). Dispersal among local communities does not reduce historical contingencies during metacommunity assembly. *Oikos*, 124(10), 1327-1336.
9. Caporaso, J. G., Kuczynski, J., Stombaugh, J., Bittinger, K., Bushman, F. D., Costello, E. K., et al. (2010). QIIME allows analysis of high-throughput community sequencing data. *Nature methods*, 7(5), 335-336.
10. Ding, T., Schloss, P. D. (2014). Dynamics and associations of microbial community types across the human body. *Nature*, 509(7500), 357-360.
11. Thompson, L. R., Sanders, J. G., McDonald, D., Amir, A., Ladau, J., Locey, K. J., et al. (2017). A communal catalogue reveals Earth's multiscale microbial diversity. *Nature*, 551(7681), 457-463.
12. Bolyen, E., Rideout, J. R., Dillon, M. R., Bokulich, N. A., Abnet, C. C., Al-Ghalith, G. A., et al. (2019). Reproducible, interactive, scalable and extensible microbiome data science using QIIME 2. *Nature biotechnology*, 37(8), 852-857.
13. Costello, E. K., Stagaman, K., Dethlefsen, L., Bohannan, B. J., Relman, D. A. (2012). The application of ecological theory toward an understanding of the human microbiome. *Science*, 336(6086), 1255-1262.

14. Widder, S., Allen, R. J., Pfeiffer, T., Curtis, T. P., Wiuf, C., Sloan, W. T., et al. (2016). Challenges in microbial ecology: building predictive understanding of community function and dynamics. *The ISME journal*, 10(11), 2557-2568.
15. Sommer, F., Anderson, J. M., Bharti, R., Raes, J., Rosenstiel, P. (2017). The resilience of the intestinal microbiota influences health and disease. *Nature Reviews Microbiology*, 15(10), 630-638.
16. Carding, S., Verbeke, K., Vipond, D. T., Corfe, B. M., Owen, L. J. (2015). Dysbiosis of the gut microbiota in disease. *Microbial ecology in health and disease*, 26(1), 26191.
17. Kelly C. P., LaMont J. T. (2008). Clostridium difficile—more difficult than ever. *New England Journal of Medicine*, 359 : 1932-1940, 2008.
18. Britton, R. A., Young, V. B. (2014). Role of the intestinal microbiota in resistance to colonization by Clostridium difficile. *Gastroenterology*, 146(6), 1547-1553.
19. Bakken, J. S., Borody, T., Brandt, L. J., Brill, J. V., Demarco, D. C., Franzos, M. A., et al. (2011). Treating Clostridium difficile infection with fecal microbiota transplantation. *Clinical Gastroenterology and Hepatology*, 9(12), 1044-1049.
20. Rillig, M. C., Antonovics, J., Caruso, T., Lehmann, A., Powell, J. R., Veresoglou, S. D., et al. (2015). Interchange of entire communities: microbial community coalescence. *Trends in Ecology and Evolution*, 30(8), 470-476.
21. Castledine, M., Sierocinski, P., Padfield, D., Buckling, A. (2020). Community coalescence: an eco-evolutionary perspective. *Philosophical Transactions of the Royal Society B*, 375(1798), 20190252.
22. Mueller, U. G., Sachs, J. L. (2015). Engineering microbiomes to improve plant and animal health. *Trends in microbiology*, 23(10), 606-617.
23. Sbahi, H., Di Palma, J. A. (2016). Faecal microbiota transplantation: applications and limitations in treating gastrointestinal disorders. *BMJ open gastroenterology*, 3(1).
24. Toju, H., Abe, M. S., Ishii, C., Hori, Y., Fujita, H., Fukuda, S. (2020). Scoring Species for Synthetic Community Design: Network Analyses of Functional Core Microbiomes. *Frontiers in microbiology*, 11, 1361.
25. May, R. M. (1977). Thresholds and breakpoints in ecosystems with a multiplicity of stable states. *Nature*, 269(5628), 471-477.
26. Scheffer, M., Carpenter, S., Foley, J. A., Folke, C., Walker, B. (2001). Catastrophic shifts in ecosystems. *Nature*, 413(6856), 591.
27. Beisner, B. E., Haydon, D. T. Cuddington, K. Alternative stable states in ecology. *Frontiers in Ecology and the Environment,* 1, 376–382 (2003).
28. Scheffer, M., Jeppesen, E. (2007). Regime shifts in shallow lakes. *Ecosystems*, 10(1), 1-3.

29. Walker, B., Holling, C. S., Carpenter, S., Kinzig, A. (2004). Resilience, adaptability and transformability in social–ecological systems. *Ecology and society*, 9(2).
30. Gibson, T. E., Carey, V., Bashan, A., Hohmann, E. L., Weiss, S. T., Liu, Y. Y. (2017). On the Stability Landscape of the Human Gut Microbiome: Implications for Microbiome-based Therapies. *bioRxiv*, 176941.
31. Shaw, L. P., Bassam, H., Barnes, C. P., Walker, A. S., Klein, N., Balloux, F. (2019). Modelling microbiome recovery after antibiotics using a stability landscape framework. *The ISME journal*, 13(7), 1845-1856.
32. Weatherby, A. J., P. H. Warren, R. Law. (1998). Coexistence and collapse: an experimental investigation of the persistent communities of a protist species pool. *Journal of Animal Ecology* 67, 554–566.
33. Law, R., A. J. Weatherby, P. H. Warren. (2000). On the invasibility of persistent protist communities. *Oikos*, 88, 319–326.
34. Warren, P. H., Law, R., Weatherby, A. J. (2003). Mapping the assembly of protist communities in microcosms. *Ecology*, 84(4), 1001-1011.
35. Law, R., Morton, R. D. (1993). Alternative permanent states of ecological communities. *Ecology*, 74(5), 1347-1361.
36. Capitán, J. A., Cuesta, J. A., Bascompte, J. (2011). Statistical mechanics of ecosystem assembly. *Physical Review Letters*, 103(16), 168101.
37. Lahti, L., Salojärvi, J., Salonen, A., Scheffer, M., De Vos, W. M. (2014). Tipping elements in the human intestinal ecosystem. *Nature communications*, 5(1), 1-10.
38. Becker, O. M., Karplus, M. (1997). The topology of multidimensional potential energy surfaces: Theory and application to peptide structure and kinetics. *The Journal of chemical physics*, 106(4), 1495-1517.
39. Wales, D. J., Miller, M. A., Walsh, T. R. (1998). Archetypal energy landscapes. *Nature*, 394(6695), 758.
40. Watanabe, T., Hirose, S., Wada, H., Imai, Y., Machida, T., Shirouzu, I., et al. (2014a). Energy landscapes of resting-state brain networks. *Frontiers in Neuroinformatics*, 8, 12.
41. Phillips, S. J., Dudík, M., Schapire, R. E. (2004). A maximum entropy approach to species distribution modeling. In Proceedings of the twenty-first international conference on Machine learning (p. 83).
42. Phillips, S. J., Anderson, R. P., Schapire, R. E. (2006). Maximum entropy modeling of species geographic distributions. *Ecological modelling*, 190(3-4), 231-259.
43. Schneidman, E., Berry, M. J., Segev, R., Bialek, W. (2006). Weak pairwise correlations imply strongly correlated network states in a neural population. *Nature*, 440(7087), 1007-1012.

44. Azaele, S., Muneepeerakul, R., Rinaldo, A., Rodriguez-Iturbe, I. (2010). Inferring plant ecosystem organization from species occurrences. *Journal of theoretical biology*, 262(2), 323-329.
45. Araujo, M. B., Luoto M. (2007). The importance of biotic interactions for modelling species distributions under climate change. *Global Ecology and Biogeography*, 16, 743–753.
46. Harris, D. J. (2016). Inferring species interactions from co - occurrence data with Markov networks. *Ecology*, 97(12), 3308-3314.
47. Jaynes, E.T., (1982). On the rationale of maximum-entropy methods. Proc. IEEE 70, 939–952.
48. Harte, J., & Newman, E. A. (2014). Maximum information entropy: a foundation for ecological theory. Trends in ecology & evolution, 29(7), 384-389.
49. Elith, J., H. Graham, C., P. Anderson, R., Dudík, M., Ferrier, S., Guisan, A., et al. (2006). Novel methods improve prediction of species' distributions from occurrence data. *Ecography*, 29(2), 129-151.
50. Kissling, W. D., Dormann, C. F., Groeneveld, J., Hickler, T., Kühn, I., McInerny, G. J., et al. (2012). Towards novel approaches to modelling biotic interactions in multispecies assemblages at large spatial extents. *Journal of Biogeography*, 39(12), 2163-2178.
51. Ockendon, N., Baker, D. J., Carr, J. A., White, E. C., Almond, R. E., Amano, T., et al. (2014). Mechanisms underpinning climatic impacts on natural populations: altered species interactions are more important than direct effects. *Global change biology*, 20(7), 2221-2229.
52. Thuiller, W., Pollock, L. J., Gueguen, M., Münkemüller, T. (2015). From species distributions to meta - communities. *Ecology letters*, 18(12), 1321-1328.
53. Barner, A. K., Coblentz, K. E., Hacker, S. D., Menge, B. A. (2018). Fundamental contradictions among observational and experimental estimates of non - trophic species interactions. *Ecology*, 99(3), 557-566.
54. Freilich, M. A., Wieters, E., Broitman, B. R., Marquet, P. A., Navarrete, S. A. (2018). Species co - occurrence networks: Can they reveal trophic and non - trophic interactions in ecological communities? *Ecology*, 99(3), 690-699.
55. Meier, E. S., Kienast, F., Pearman, P. B., Svenning, J. C., Thuiller, W., Araújo, M. B., et al. (2010). Biotic and abiotic variables show little redundancy in explaining tree species distributions. *Ecography*, 33(6), 1038-1048.
56. Leach, K., Montgomery, W. I., Reid, N. (2016). Modelling the influence of biotic factors on species distribution patterns. *Ecological Modelling*, 337, 96-106.
57. Barbaro, L., Allan, E., Ampoorter, E., Castagneyrol, B., Charbonnier, Y., De Wandeler, H., et al. (2019). Biotic predictors complement models of bat and bird

responses to climate and tree diversity in European forests. *Proceedings of the Royal Society B*, 286(1894), 20182193.
58. Clark, N. J., Wells, K., Lindberg, O. (2018). Unravelling changing interspecific interactions across environmental gradients using Markov random fields. *Ecology*, 99(6), 1277-1283.
59. Watanabe, T., Masuda, N., Megumi, F., Kanai, R., Rees, G. (2014b). Energy landscape and dynamics of brain activity during human bistable perception. *Nature Communications*, 5, 4765.
60. Ezaki, T., Watanabe, T., Ohzeki, M., Masuda, N. (2017). Energy landscape analysis of neuroimaging data. *Philosophical Transactions of the Royal Society A: Mathematical, Physical and Engineering Sciences*, 375(2096), 20160287.
61. Watanabe, T., Rees, G. (2017). Brain network dynamics in high- functioning individuals with autism. *Nature Communications*, 8, 16048.
62. Ezaki, T., Sakaki, M., Watanabe, T., Masuda, N. (2018). Age–related changes in the ease of dynamical transitions in human brain activity. *Human brain mapping*, 39(6), 2673-2688.
63. Nguyen, H. C., Zecchina, R., Berg, J. (2017). Inverse statistical problems: from the inverse Ising problem to data science. *Advances in Physics*, 66(3), 197-261.
64. Shipley, B., Vile, D., & Garnier, É. (2006). From plant traits to plant communities: a statistical mechanistic approach to biodiversity. *Science*, 314(5800), 812-814.
65. Franklin, J. (2010). Mapping species distributions: spatial inference and prediction. Cambridge University Press.
66. Parisien, M. A., Moritz, M. A. (2009). Environmental controls on the distribution of wildfire at multiple spatial scales. *Ecological Monographs*, 79(1), 127-154.
67. Harte, J. (2011). Maximum entropy and ecology: a theory of abundance, distribution, and energetics. OUP Oxford.
68. Staniczenko, P. P., Sivasubramaniam, P., Suttle, K. B., Pearson, R. G. (2017). Linking macroecology and community ecology: refining predictions of species distributions using biotic interaction networks. *Ecology letters*, 20(6), 693-707.
69. Gilks, W. R., Richardson, S., Spiegelhalter, D. J. (1996). Introducing Markov chain Monte Carlo. Markov chain Monte Carlo in practice. Chapman & Hall .
70. Bickel, P., K. Doksum. (1977). Mathematical Statistics: Basic Ideas and Selected Topics. San Francisco: Holden-Day.
71. Murphy, K. P. (2012). Machine Learning: A Probabilistic Perspective. The MIT Press.
72. Harris, D. J. (2015). Multi-Process Statistical Modeling of Species' Joint Distributions. University of California, Davis.

73. Lee, J. D., Hastie, T. J. (2015). Learning the structure of mixed graphical models. *Journal of Computational and Graphical Statistics*, 24(1), 230-253.
74. Robbins, H., S. Monro. 1951. A Stochastic Approximation Method. *The Annals of Mathematical Statistics* 22:400–407.
75. Salakhutdinov, R., and G. Hinton. (2012). An efficient learning procedure for deep Boltzmann machines. *Neural Computation* 24:1967–2006.
76. Younes, L. 1999. On the convergence of Markovian stochastic algorithms with rapidly de- creasing ergodicity rates. *Stochastics: An International Journal of Probability and Stochastic Processes* 65:177–228.
77. Hinton, G. E. (2012). A practical guide to training restricted Boltzmann machines. In Neural networks: Tricks of the trade (pp. 599-619). Springer, Berlin, Heidelberg.
78. Gilpin, M. E., Case, T. J. (1976). Multiple domains of attraction in competition communities. *Nature*, 261(5555), 40-42.
79. Wilson, W. G., Deroos, A. M., McCauley, E. (1993). Spatial instabilities within the diffusive Lotka-Volterra system: individual-based simulation results. *Theoretical population biology*, 43(1), 91-127.
80. Keymer, J. E., Marquet, P. A., Velasco-Hernández, J. X., Levin, S. A. (2000). Extinction thresholds and metapopulation persistence in dynamic landscapes. *The American Naturalist*, 156(5), 478-494.
81. Gerber, G. K. (2014). The dynamic microbiome. *FEBS letters*, 588(22), 4131-4139.
82. Scheffer, M., Carpenter, S. R., Lenton, T. M., Bascompte, J., Brock, W., Dakos, V., et al. (2012). Anticipating critical transitions. *Science*, 338(6105), 344-348.
83. Scheffer, M., Carpenter, S. R., Dakos, V., van Nes, E. H. (2015). Generic indicators of ecological resilience: inferring the chance of a critical transition. *Annual Review of Ecology, Evolution, and Systematics*, 46, 145-167.
84. Chase, J.M. (2014). Spatial scale resolves the niche versus neutral theory debate. *Journal of vegetation science*, 25, 319-322.
85. Viana, D.S., Chase, J.M. (2019). Spatial scale modulates the inference of metacommunity assembly processes. *Ecology*, 100, e02576. https://doi.org/10.1002/ecy.2576
86. Legendre, P., Mi, X., Ren, H., Ma, K., Yu, M., Sun, I.F., et al. (2009). Partitioning beta diversity in a subtropical broad - leaved forest of China. *Ecology*, 90, 663-674.
87. Meynard, C.N., Lavergne, S., Boulangeat, I., Garraud, L., Van Es, J., Mouquet, N., et al. (2013). Disentangling the drivers of metacommunity structure across spatial scales. *Journal of biogeography*, 40, 1560-1571.
88. D'Amen, M., Mod, H. K., Gotelli, N. J., Guisan, A. (2018). Disentangling biotic interactions, environmental filters, and dispersal limitation as drivers of species co - occurrence. *Ecography*, 41, 1233-1244.

89. Mertes, K., Jetz, W. (2018). Disentangling scale dependencies in species environmental niches and distributions. *Ecography*, 41, 1604-1615.
90. Langille, M. G., Meehan, C. J., Koenig, J. E., Dhanani, A. S., Rose, R. A., Howlett, S. E., et al. (2014). Microbial shifts in the aging mouse gut. *Microbiome*, 2(1), 50.
91. Holling, C. S. (1996). Engineering resilience versus ecological resilience. In Engineering within Ecological Constraints, ed. PC Schulze, pp. 31–44. Washington, DC: Natl. Acad. Press.
92. Weiher, E., Keddy, P. (Eds.). (2001). Ecological assembly rules: perspectives, advances, retreats. Cambridge University Press.
93. Lockwood, J. L., Samuels, C. L. (2004). Assembly models and the practice of restoration. In Assembly Rules and Restoration Ecology: Bridging the Gap Between Theory and Practice, ed. VM Temperton, RJ Hobbs, T Nuttle, S Halle, pp. 55–70. Washington, DC: Island Press.
94. Suding, K. N., Gross, K. L., Houseman, G. R. (2004). Alternative states and positive feedbacks in restoration ecology. *Trends in Ecology and Evolution*, 19, 46–53.
95. Wilsey, B. J., Barber, K., Martin, L. M. (2015). Exotic grassland species have stronger priority effects than natives regardless of whether they are cultivated or wild genotypes. *New Phytologist*, 205, 928–37.
96. Young, T. P., Petersen, D. A., Clary, J. J. (2005). The ecology of restoration: historical links, emerging issues and unexplored realms. *Ecology Letters*, 8, 662–73.
97. Young, T. P., Zefferman, E. P., Vaughn, K. J., Fick, S. (2015). Initial success of native grasses is contingent on multiple interactions among exotic grass competition, temporal priority, rainfall, and site effects. *AoB PLANTS,* 7, 081.
98. Verbruggen, E., van der Heijden, M. G., Rillig, M. C., Kiers, E. T. (2013). Mycorrhizal fungal establishment in agricultural soils: factors determining inoculation success. *New Phytologist,* 197, 1104–1109.
99. Toju, H., Peay, K. G., Yamamichi, M., Narisawa, K., Hiruma, K., Naito, K., et al. (2018). Core microbiomes for sustainable agroecosystems. *Nature Plants*, 4(5), 247-257.
100. Fierer, N., Ferrenberg, S., Flores, G. E., González, A., Kueneman, J., Legg, T., et al. (2012). From animalcules to an ecosystem: application of ecological concepts to the human microbiome. *Annual Review of Ecology, Evolution, and Systematics*, 43, 137-155.
101. Lam, L. H., Monack, D. M. (2014). Intraspecies competition for niches in the distal gut dictate transmission during persistent Salmonella infection. *PLoS pathogens*, 10(12), e1004527.

102. Devevey, G., Dang, T., Graves, C. J., Murray, S., Brisson, D. (2015). First arrived takes all: inhibitory priority effects dominate competition between co-infecting Borrelia burgdorferi strains. *BMC microbiology*, 15(1), 61.
103. Smits, L. P., Bouter, K. E., de Vos, W. M. et al. (2013). Therapeutic potential of fecal microbiota transplantation. *Gastroenterology* 145:946–53.
104. Li, S. S., Zhu, A., Benes, V., Costea, P. I., Hercog, R., Hildebrand, F., et al. (2016). Durable coexistence of donor and recipient strains after fecal microbiota transplantation. *Science* 352, 586–586.
105. Shetty, S. A., Hugenholtz, F., Lahti, L., Smidt, H., de Vos, W. M. (2017). Intestinal microbiome landscaping: insight in community assemblage and implications for microbial modulation strategies. *FEMS microbiology reviews*, 41(2), 182-199.
106. Karczewski, J., Poniedziałek, B., Adamski, Z., Rzymski, P. (2014). The effects of the microbiota on the host immune system. *Autoimmunity*, 47(8), 494-504.
107. Cox, L. M., Blaser, M. J. (2015). Antibiotics in early life and obesity. *Nature Reviews Endocrinology*, 11(3), 182.
108. Tang, A. T., Choi, J. P., Kotzin, J. J., Yang, Y., Hong, C. C., Hobson, N., et al. (2017). Endothelial TLR4 and the microbiome drive cerebral cavernous malformations. *Nature*, 545(7654), 305.
109. Hartig, F. Dormann, C.F. (2013). Does model-free forecasting really outperform the true model? *Proceedings of the National Academy of Science*, 110, E3975-E3975.
110. Perretti, C. T., Munch, S. B., Sugihara, G. (2013a) Model-free forecasting outperforms the correct mechanistic model for simulated and experimental data. *Proceedings of the National Academy of Science*, 110, 5253-5257.
111. Perretti, C. T., Munch, S. B., Sugihara, G. (2013b). Reply to Hartig and Dormann: the true model myth. *Proceedings of the National Academy of Science*, 110, E3976-E3977.
112. DeAngelis, D. L., Yurek, S. (2015). Equation-free modeling unravels the behavior of complex ecological systems. *Proceedings of the National Academy of Sciences*, 112, 3856-3857.
113. Cubitt, T. S., Eisert, J., Wolf, M. M. (2012). Extracting dynamical equations from experimental data is NP hard. *Physical Review Letters*, 108, 120503.
114. Wootton, J. T. (2001). Prediction in complex communities: analysis of empirically derived Markov models. *Ecology*, 82(2), 580-598.
115. Chang, W. K., VanInsberghe, D., Kelly, L. (2020). Towards a potential landscape framework of microbiome dynamics. *bioRxiv*, 584201.

116. Morton, R. D., Law, R. (1997). Regional species pools and the assembly of local ecological communities. *Journal of Theoretical Biology*, 187, 321–331.
117. Sugihara, G., May, R., Ye, H., Hsieh, C. H., Deyle, E., Fogarty, M., et al. (2012). Detecting causality in complex ecosystems. *Science*, 338(6106), 496-500.
118. Runge, J., Nowack, P., Kretschmer, M., Flaxman, S., Sejdinovic, D. (2019). Detecting and quantifying causal associations in large nonlinear time series datasets. *Science Advances*, 5(11), eaau4996.
119. Long, Z.T. and Karel, I. (2002) Resource specialization determines whether history influences community structure. *Oikos*, 96, 62–9.
120. Chase, J.M and Leibold, M.A. (2003) Ecological Niches: Linking Classical and Contemporary Approaches. University of Chicago Press, Chicago, IL
121. Mouquet, N., Lagadeuc, Y., Devictor, V., Doyen, L., Duputié, A., Eveillard, D., et al. (2015). Predictive ecology in a changing world. *Journal of Applied Ecology*, 52(5), 1293-1310.

Appendix A: Parameter values and models used to generate data sets

The interaction matrix used to generate a data set in *Analysis of a competitive Lotka-Volterra system, Energy landscape of the LV system, Emulating community assembly dynamics*, are in Table S1.

The response vector b in *Energy landscape across environmental gradient* is:

$$b = (0.26, -0.39, 0.16, 0.36, 0, -0.43, 0.28, 0.02, -0.45, -0.46, -0.32, -0.41, 0.14, 0.18, -0.01)$$

In *Benchmarking*, the interaction matrix A was generated so that the connectance $c_A = 0.5$, and its non-zero diagonal elements (interspecific competition) were drawn from a normal distribution with a mean $\mu_A = 0.6$ and variance $\sigma_A = 0.2$. We fixed the diagonal elements (intraspecific interaction) as $a_{ii} = 1$. To obtain the result under type II functional response (G in Fig. 7), we extended the eq.(5) as

$$dx_i = x_i\left(1 - \Sigma_{\mathrm{i}} \frac{a_{ij}x_i}{0.5 + \Sigma_{\mathrm{j}} a_{ij}x_i} + \Sigma b_i \epsilon_i\right),$$

and to obtain data set with noise (H in Fig. 7), we used,

$$dx_i = x_i\left(1 - \Sigma_{\mathrm{i}} \frac{a_{ij}x_i}{0.5 + \Sigma_{\mathrm{j}} a_{ij}x_i} + \eta_{\mathrm{i}}\right).$$

Here, η_{i} is assumed to be the i.i.d noise drawn from a normal distribution of mean 0 and s.d. 0.1 (H).

Table S1. Elements of A.

1	0	0.58	0.62	0	0.61	0.29	0	0	0.55	0.69	0.54	0.66	0	0	0
0.8	1	0	0.53	0.61	0.65	0	0.78	0	0.58	0.74	0.72	0	0.52	0.62	0
0	0	1	0.61	0.68	0	0	0	0	0	0	0.45	0.62	0.67	0.7	0
0.33	0.56	0.58	1	0.51	0.5	0.65	0.52	0	0.55	0	0	0.61	0	0.54	0.48
0.77	0	0.63	0.57	1	0.67	0.55	0.61	0	0.63	0	0.57	0	0.48	0.52	0.86
0	0	0.58	0.43	0	1	0.47	0.75	0.53	0	0.49	0.49	0.45	0	0.51	0
0.54	0	0	0.61	0.7	0	1	0	0.4	0	0.63	0	0.79	0.55	0	0

0	0	0.6	0.56	0.43	0	0.76	1	0	0	0.51	0.9	0.59	0.77	0.52	0
0.55	0	0	0.66	0.63	0	0.61	0	1	0	0.44	0	0	0	0.48	0.39
0	0.38	0.56	0.55	0	0.47	0.56	0.76	0	1	0	0	0	0.54	0.62	0
0.44	0	0.49	0	0.71	0.52	0	0.47	0.77	0	1	0.75	0.84	0	0.67	0.75
0.58	0.33	0	0.47	0.68	0.46	0	0.42	0.61	0.6	0.61	1	0.63	0.7	0.69	0
0.7	0	0	0.57	0	0	0.62	0	0	0.78	0.63	0.67	1	0	0	0.51
0.54	0.74	0	0	0.51	0	0.78	0.49	0	0	0.71	0.44	0.43	1	0.64	0
0.45	0	0.62	0	0.54	0.73	0	0.47	0.67	0.77	0	0.7	0.69	0.53	1	0
0.81	0.46	0	0.67	0.38	0.65	0	0	0.55	0.85	0.76	0	0.58	0	0.55	1